DIETARY MODULATION OF INFLAMMATION-MEDIATED EFFECTS ON SKELETAL BIOLOGY

A Dissertation

by

SARAH ELIZABETH LITTLE

Submitted to the Office of Graduate and Professional Studies of
Texas A&M University
in partial fulfillment of the requirements for the degree of

DOCTOR OF PHILOSOPHY

Chair of Committee,	Susan Bloomfield
Committee Members,	J. Timothy Lightfoot
	Michael Massett
	John Ford
Head of Department,	Melinda Sheffield-Moore

May 2020

Major Subject: Kinesiology

ABSTRACT

Chronic inflammation leads to bone loss and fragility. Signaling of pro-inflammatory cytokines, like tumor necrosis factor-alpha (TNFα), is integral to promote bone resorption. Dietary modulation of pro-inflammatory cytokines is a therapeutic target for disorders associated with chronic inflammation, including space-relevant radiation exposure and diet-induced obesity (DIO), though much remains poorly understood. As such, we seek to investigate whether an anti-inflammatory diet can reduce radiation-mediated damage and whether diet and microbiota supplementation can reverse the negative effects of a pro-inflammatory diet on bone.

We assessed the efficacy of a diet high in omega-3 fatty acids in mitigating radiation-induced bone loss via reductions in inflammatory cytokines in bone osteocytes and serum. Interestingly, we failed to detect a negative impact of radiation exposure on cancellous and cortical bone parameters, despite increased serum levels of TNFα with radiation exposure. A high omega-3 fatty acid diet mitigated the radiation-induced increase in serum levels of TNFα. High omega-3-fed mice exhibited improved cancellous and cortical microarchitecture and geometry at 8 weeks post-exposure to ^{56}Fe and γ radiation, with improvements occurring at higher radiation doses. Though we did not detect the expected impact of radiation on bone parameters, mitigation of inflammatory cytokines via an anti-inflammatory diet resulted in modest improvements in bone outcomes and reduced systemic inflammation, as assessed by serum TNFα.

In the second experiment, we assessed whether altering dietary intake from a high fat, high sugar (HFS) to a low-fat diet, with or without fecal microbial transplants (FMT) rescued bone integrity in diet-induced obesity. Contrary to our expectations, HFS feeding promoted bone anabolism and improved femur structural properties with no detectable inflammatory impact, suggesting exercise is protective against systemic inflammation. HFS-fed mice did not improve femur material properties, nor femoral neck strength, suggesting improved bone quantity, but not quality. FMT treatment exhibited a differential impact on femur material properties that should be investigated further.

Together, our results suggest that dietary modulation of inflammatory cytokines may be effective against negative bone impacts related to systemic inflammation; however, in the context of chronic inflammation and DIO, exercise appears to outweigh the detrimental impact of HFS-induced inflammation on bone.

DEDICATION

To my dog, Jackson.

ACKNOWLEDGEMENTS

I would like to thank my committee chair, Dr. Bloomfield, for many things – namely, taking me on as her student and providing countless pieces of advice and mentorship. I would also like to thank my committee members, Dr. Lightfoot, Dr. Ford, and Dr. Massett, as well as Dr. Charles, an unofficial member and valued advisor, for their guidance and support throughout my development as a scientist. I truly could not have gotten to where I am without the support and mentorship of all of you.

Thank you to all of my friends and fellow doctoral students at Texas A&M University. My five years in College Station would not have been the same without you all. Thank you for brightening up my days when the rollercoaster that is science got me down and celebrating with me when times were good. Special thanks to Selina Uranga and Marble (Jackson's best friend and my favorite roommate), Bri Breidenbach, Pat Ryan, Dylan Holly, Nathan Keller, and Kalen Johnson.

Lastly, I'd like to thank my almost husband, Ayland Letsinger, for everything: for designing, running, and letting me steal the skeletons from your dissertation for mine; for the countless words of encouragement; for always believing in me, especially when I didn't believe in myself; for being the first person to tell me I should do research and that I could do research, even if it was only to keep me around. I can't wait to collaborate with you in the future and to see where life takes us!

CONTRIBUTORS AND FUNDING SOURCES

Contributors

This work was supervised by a dissertation committee consisting of Dr. Susan Bloomfield [advisor] and Dr. J. Timothy Lightfoot of the Department of Health and Kinesiology, Dr. John Ford of the Department of Nuclear Engineering, and Dr. Michael Massett of the Department of Kinesiology and Sports Management at Texas Tech University, as well as Dr. John Charles, an unofficial member and valued advisor.

All animal protocol work and tissue samples analyzed for Chapter 2 were provided by Dr. Nancy Turner, of the Department of Nutrition and Food Science, and her doctoral students. Animal protocol work and tissue samples analyzed for Chapter 3 were provided by Dr. J. Timothy Lightfoot and Dr. Ayland Letsinger of the Department of Health and Kinesiology. Special thanks to Drs. Larry Suva, Dana Gaddy, Ken Muneoka, Matthew Allen, Corinne Metzger, and Harry Hogan and their students, for equipment use and assistance with specialized analyses.

All other work conducted for the dissertation was completed by the student independently, in addition to participation in animal protocol work for Chapter 3.

Funding Sources

Graduate study was supported by a graduate teaching assistantship from Texas A&M University and a graduate research assistantship co-funded by grants from Dr. Susan Bloomfield, Dr. Jerry Feng, and Dr. Bonnie Dunbar.

This work was also made possible in part by grants from the National Aeronautics and Space Administration awarded to both ND Turner and SA Bloomfield, the Sydney & J.L. Huffines Institute for Sports Medicine and Human Performance, the Omar Smith Endowment, and the College of Education and Human Development. Its contents are solely the responsibility of the authors and do not necessarily represent the official views of the awarding offices.

TABLE OF CONTENTS

Page

LIST OF FIGURES

Page

LIST OF TABLES

Page

1. INTRODUCTION

1.1. Osteoimmunology: Inflammation-Mediated Effects on Bone Biology

Osteoimmunology is the study of the intersection between the skeletal system and the immune system. There exists a reciprocal relationship between these two systems, whereby several inflammatory cytokines are required for bone homeostasis and factors secreted by bone cells are essential for the proper development and function of many immune cells. The immune system is a key player in the maintenance of bone mass, particularly in pathological conditions characterized by a high degree of systemic inflammation (90) like osteoporosis, inflammatory bowel disease, Crohn's disease, type 2 diabetes, diet-induced obesity and radiation exposure (1, 14, 76, 104).

Inflammation can lead to bone loss and fragility and has been associated with increased incidence of fracture (6, 51, 76, 104). Mechanistically, inflammation leads to an excess production of several inflammatory cytokines, like tumor necrosis factor alpha (TNFα), which potently stimulate bone resorption (90). Maintenance of bone mass is dependent upon the coupling of bone formation and resorption, both temporally and spatially (42). Chronic inflammation leads to the uncoupling of bone formation and resorption, in favor of resorption, which ultimately results in bone loss through the direct effects of inflammation and poor nutrition, among others (42). This proposal will focus on the inflammation-related bone loss induced by radiation exposure and diet-induced obesity, as well as the ability for diet to mitigate inflammation-derived damage to bone.

1.1.1. Fundamentals of Bone Microarchitecture & Biology

1.1.1.1. Bone Microarchitecture: Impacts on Mechanical Strength

Two main types of bone exist, each with specific functions and properties. Cortical bone serves as the thick, dense shell and accounts for the majority of skeletal bone mass. Cortical bone is the primary component of the diaphysis, or shafts, of long bones, and surrounds cancellous bone at the metaphysis, or ends, of long bones and in the vertebrae. Blood vessels and nerve fibers pass through cortical bone via Haversian canals, which results in small degree of porosity (~3-5%) (15). Mechanically, cortical bone is essential for load bearing and provides strength and stiffness, which are key

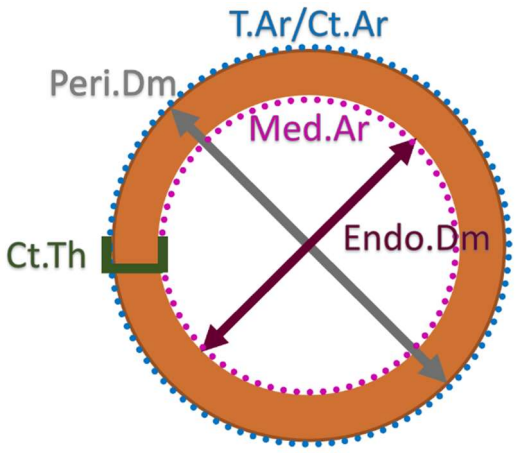

Figure 1-1. Cartoon depicting cross-sectional components of cortical microarchitecture, specifically, T.Ar/Ct.Ar, Med.Ar, Peri.Dm, Endo.Dm, and Ct.Th.

factors for bone strength (15, 97). The geometry of cortical bone is a primary determinant of strength and has several components (Figure 1-1). Total area (T.Ar) or cortical area (Ct.Ar) denotes the total cross-sectional area of cortical shell; an increase in T.Ar/Ct.Ar leads to a strength increase of r^4. For example, it's easy to snap a thin stick in

half, but a stick with a slightly larger cross-sectional area is exponentially harder to snap. Medullary area (Med.Ar) is the area inside of the cortical shell, denoted in the thick orange band. Periosteal diameter (Peri.Dm) is the diameter of the cortical cross-section and endocortical diameter (Endo.Dm) is the diameter of the medullary area. Cortical thickness (Ct.Th) is the width of the cortical shell; an increase in Ct.Th is typically associated with an increase in strength. Cortical porosity (*not shown in Fig. 1-1*) is another component of cortical bone and denotes the number of pores embedded in the cortical shell; an increase in cortical porosity is associated with a decrease in bone quality and ultimately bone strength. With aging and inflammation, Ct.Th declines, cortical porosity increases, and Ct.Ar and Med.Ar increase as a compensatory mechanism to maintain some mechanical strength (Fig. 1-2). Long-term obesity typically has the same effect on cortical geometry, though short-term obesity has been associated with increased Ct.Th (Figure 1-2). Mechanical testing of cortical bone yields

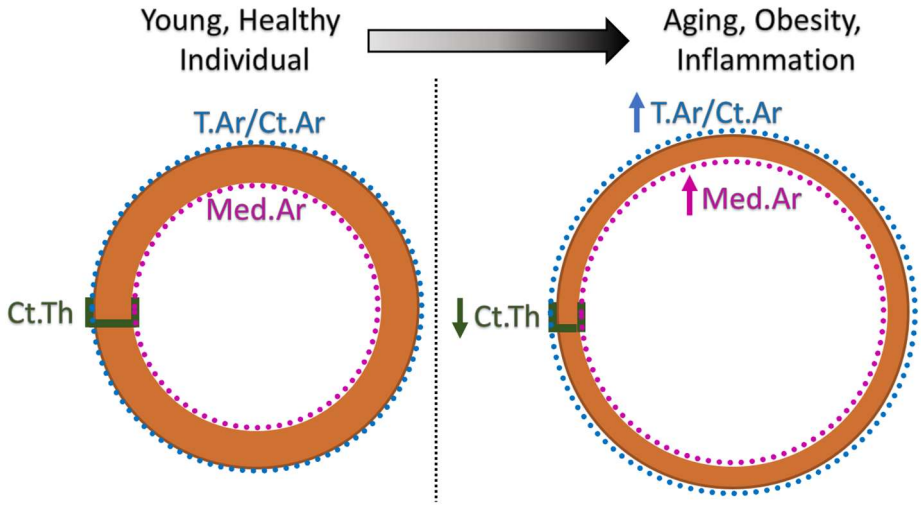

Figure 1-2. Changes in cortical microarchitecture with aging, obesity, and inflammation.

data on both structural (size and geometry dependent) and material (tissue level, size independent) properties of bone. Improvements in structural properties coincide with improvements in cortical geometry; while improvements in material properties coincide with improvements in tissue and/or bone quality.

Cancellous bone, also called trabecular or spongy bone, is porous and serves to internally re-direct load to the cortical shell (97, 115). In the long bones, like the femur and tibia, cancellous bone is located at the metaphysis and houses mesenchymal and hematopoietic stem cells. At a micro-structural level, cancellous bone is composed of an

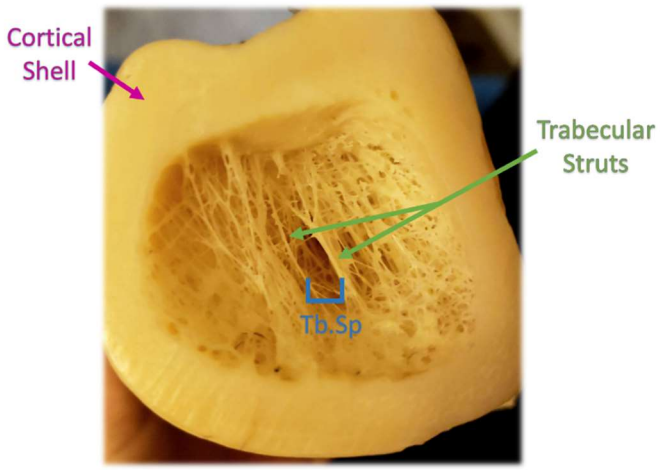

Figure 1-3. Cross-sectional image, oriented towards the metaphysis, of components of cancellous microarchitecture.

enmeshed array of plates and rods, termed trabeculae, creating a "spongy" appearance. The microarchitectural parameters of cancellous bone are integral for mechanical strength, particularly the number, thickness, and spacing of trabeculae (Figure 1-3). Together, these parameters determine overall cancellous bone volume. Trabecular

number (Tb.N) is the number of trabecular struts and trabecular thickness (Tb.Th) is the average width of trabeculae within the metaphyseal compartment. An increase in Tb.N and Tb.Th is indicative of an increase in bone volume or total bone mass, which is associated with increased strength. Trabecular spacing (Tb.Sp) is the average distance between trabeculae; a decrease in Tb.Sp is positively related to increased bone volume and strength. Changes in Tb.N, Tb.Th and Tb.Sp are the mechanism by which bone volume or bone mass can increase. Cancellous bone volume is reported as bone volume relative to total volume of the metaphyseal space (BV/TV). An increase in BV/TV, Tb.N and Tb.Th and a decrease in Tb.Sp would describe an improvement in cancellous microarchitecture. With aging and inflammation, BV/TV, Tb.N, and Tb.Th decrease and Tb.Sp increase, so cancellous microarchitecture is diminished. Similar to cortical microarchitecture, short-term obesity typically improves cancellous microarchitecture, while long-term studies suggest a similar profile to aging and inflammation (Figure 1-4).

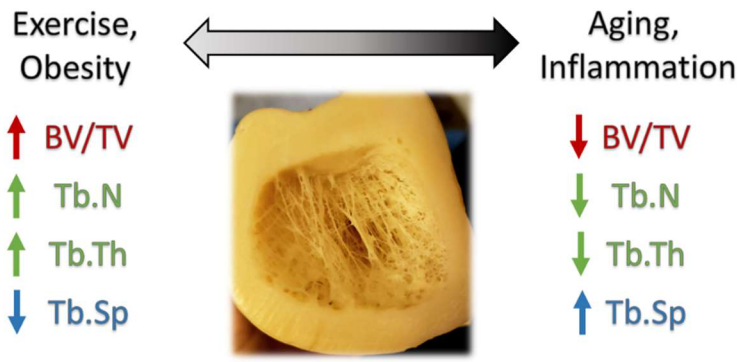

Figure 1-4. Changes in cancellous microarchitecture with exercise and obesity versus aging and inflammation.

While cortical and cancellous bone both contribute to mechanical strength of bone through different properties and parameters, overall bone strength is derived from a

combination of bone mass and bone quality. Bone quality is dependent upon four primary determinants: 1) rate of bone turnover, 2) microarchitecture and geometry, 3) material properties, specifically mineralization and collagen content (e.g. bone mineral density), and 4) accumulation of microdamage (15, 97). Of course, bone turnover, discussed below, can directly alter each of the other determinants.

Bone turnover, or bone metabolism, is the normal cycle of bone formation and resorption. In a healthy individual, bone is continuously remodeling, with rate depending on the specific bone site. Bone turnover is a tightly regulated process orchestrated by osteocytes whereby osteoclasts, or bone resorption cells, act to resorb bone in a site-specific manner, followed by osteoblasts, or bone formation cells, which lay down bone matrix for mineralization. Regulation of bone turnover, temporally and spatially, is integral for bone quality. For example, a spatial mismatch, or un-coupling, of bone formation and resorption could result in resorption of bone in area A and formation in area B, which would lead to thinning in area A and thickening in area B, altering bone microarchitecture and ultimately bone strength. With aging, inflammation, and disease, bone resorption outweighs bone formation, resulting in loss of bone mass and mechanical strength, and typically detriments in bone quality. Mechanical loading, often acquired via exercise, provides a stimulus for bone formation and can help to mitigate loss of bone mass and strength in aging and other disease states. With obesity, short-term improvements are often discovered largely due to the weight gain-induced increase in mechanical loading, while long-term, systemic inflammation can cause detriments to bone quality.

1.1.1.2. Osteoclasts

Osteoclasts are the primary cells involved in bone resorption and are derived from hematopoietic stem cells (33). Differentiation of osteoclasts from stem cell progenitors is stimulated by macrophage colony-stimulating factor and receptor activator of nuclear factor kappa-B ligand (RANKL) and inhibited by osteoprotegerin (OPG), which are discussed below (22, 109). An increase in the production of osteoclasts, or osteoclastogenesis, results in increased bone resorption and, when combined with uncoupling of bone turnover, leads to loss of bone mass. Conversely, a decrease in osteoclastogenesis can lead to increased bone mass. Several factors can act on stem cell progenitors to promote (e.g. TNFα) or inhibit differentiation of osteoclasts, as well as alter the activity and survival of osteoclasts. Osteoclast number and activity are standard metrics of bone resorption alongside measures of osteoclastogenic gene and protein expression.

1.1.1.3. Osteoblasts

Osteoblasts are the primary cells responsible for bone formation and are derived from mesenchymal stem cells (33). Osteoblasts have three potential fates after bone matrix formation is completed: 1) apoptosis, 2) bone forming cells, which are quiescent cells that line bone surfaces, and 3) osteocytes, which are discussed below. Differentiation of osteoblasts from stem cell progenitors is stimulated by the bone morphogenic protein (BMP) and Wnt signaling pathways, predominantly via runt-related transcription factor 2 (RUNX2), osterix, and β-catenin, though β-catenin can act as an inhibitor at certain stages of differentiation (19, 31). An increase in the production

of osteoblasts, or osteoblastogenesis/osteogenesis, results in increased bone formation and, when combined with uncoupling of bone turnover, leads to a gain of bone mass. Conversely, a decrease in osteogenesis can lead to decreased bone mass. Several factors can act to promote (e.g. Insulin-like Growth Factor 1 [IGF-1]) or inhibit (e.g. sclerostin) differentiation of osteoblasts, as well as alter the activity and survival of osteoblasts. Similar to osteoclasts, osteoblast number and activity, as well as osteogenic gene and protein expression are standard metrics used to quantify bone formation.

1.1.1.4. Osteocytes

Osteocytes are the master controllers of bone, coordinating the function of osteoclasts and osteoblasts, and are the most abundant bone cell (33). Osteocytes, formed when osteoblasts become trapped during bone formation and mineralization, are housed in individual caverns, called lacunae, and connect with other osteocytes via dendritic processes that extend through tunnels, called canaliculi, creating a dense network in both cortical and cancellous bone. Osteocyte regulation of osteoblasts and osteoclasts occurs in response to a number of stimuli, including mechanical signals and circulating proteins and hormones. In response to these stimuli, osteocytes can produce and secrete factors specific to the regulation of key bone processes. Bone formation is stimulated via decreases in osteocyte-derived sclerostin expression, a negative regulator of bone formation, which leads to an increase in canonical Wnt signaling and ultimately promotes differentiation of osteoblasts from mesenchymal stem cells (15). Bone resorption is stimulated via increases in the osteocyte-derived RANKL which promotes differentiation of osteoclasts from hematopoietic stem cells (34). Osteocytes also secret

osteoprotegerin (OPG), which competitively acts on RANKL binding sites on osteoclasts, and can act to decrease bone resorption (13). Many cells and factors can bind to osteocytes to induce bone formation (e.g. IGF-1) and bone resorption (e.g. TNFα).

1.2. Radiation-Induced Inflammation

1.2.1. Space-relevant Radiation Exposure

Two main types of space-relevant radiation exist: galactic cosmic radiation (GCR) and solar particle events (SPE). GCR is a type of cosmic background radiation originating from outside of the solar system. GCR is composed primarily of protons (~99%) with a small portion of high atomic number and energy (HZE) ions, such as iron (Fe) (5). Though only 1% of the total composition, HZE ions account for 41% of the dose equivalent, with ~13% from Fe ions alone (5). Estimated dose rates for GCR total about 0.4-0.8 milli-grey (mGy) per day, leading to a cumulative dose of about 1 Gy on a 400-day mission (83, 84). Conversely, a SPE is a large mass ejection from the sun, commonly referred to as a solar flare. Dose rates for a SPE vary dramatically, depending on the size of the event and protection available. For 8-24 hours of exposure, the dose rate for protons alone is about 1-2 Gy (123).

The first documentations of the deleterious impact of space-relevant radiation exposure on bone quality were performed in the 1970's on the first Mir and Sky Lab astronauts (57, 61). These early studies showed that alterations to cortical and cancellous bone occur at different rates, with cortical loss of ~1% per month and

cancellous loss of ~2-2.7% per month, though these astronauts experienced a combined impact of radiation exposure and skeletal unloading (57, 117). The magnitude and site of bone loss is dependent upon many factors, including the absorbed dose, dose rate, ion species involved, age and developmental stage of the human, and sex (78, 87, 125). Bone is affected within three days of radiation exposure via increases in osteoclast activity, though changes in gene expression occur rapidly (122). Bone loss can persist for months following irradiation and complete recovery of bone may never occur, with some parameters showing irreversible changes (58, 59, 117, 122).

Historically, radiation-induced bone loss was believed to be due to damage to the vasculature in bone, specifically Haversian canals (30, 91). While radiation exposure does result in ablation of vasculature in bone, including both marrow and Haversian canals, this is due to the swelling and vacuolization of endothelial cells (30, 91). Recent investigations into the mechanisms of bone loss have focused on bone forming cells, called osteoblasts, bone resorption cells, called osteoclasts, and master regulatory cells of bone, called osteocytes.

1.2.2. Mechanisms of Action

Space-relevant radiation exposure leads to a rapid acceleration of bone resorption activity and some suppression of bone forming osteoblasts, which results in diminished bone mineral density, strength and microarchitecture (5, 67, 124). Radiation exposure leads to decreases in osteoblast number, proliferation, differentiation and matrix formation, resulting in decreases in bone formation rates (122). Osteoclast activity and surface area are increased after irradiation, leading to increases in bone resorption (122).

The combined suppression of bone formation and activation of bone resorption causes loss of bone mineral density and strength and detrimental alterations to bone microarchitecture. Simulation of GCR via acute doses of 2 Gy or less causes rapid and dramatic loss of cancellous bone (15-20%) in rodent models (1, 5, 41, 67). Similar bone loss has also been shown in astronauts following six months on the International Space Station with exposure to an average of 0.08 to 0.16 Gy, depending on solar cycles (57, 83, 117); however, this also involves the addition of skeletal unloading, which may be additive to bone loss (1, 41, 53). Estimated dosing for an exploration class mission to mars is approximately 1 Gy of GCR (83). Combined radiation and skeletal unloading may exacerbate bone loss, though several studies report that radiation and weightlessness activate different cellular mechanisms to enact bone loss and thus the stimulus for bone loss may be saturated such that the combination has no additional impact (1, 41, 53).

Inflammation is one of the earliest responses to radiation exposure (40), with astronauts and rodents flown in space showing elevated levels of pro-inflammatory cytokines, such as Interleukin-6 (IL), IL-8, IL-10, and TNF-α (11, 23, 37). TNF-α expression is significantly increased in bone marrow within 24 hours and in homogenized cortical bone three days post-exposure to 2 Gy of gamma radiation (1). Osteoclast activity, indicative of bone resorption, and serum levels of TRAP5b, a serum marker of bone resorption, are also significantly increased three days post-exposure to 2 Gy of x-rays (122, 124). Mechanistically, TNF-α is a pro-inflammatory cytokine capable of communicating with osteoctyes and influencing both osteoclasts (52, 56) and

osteoblasts (43, 82). TNF-α is a potent stimulator of bone resorption via stimulation of osteoclastogenesis and increased RANKL production (52, 56, 82) and an inhibitor of bone formation via decreased production of osteogenic genes and differentiation factors, like RUNX2 (48), and reduced collagen synthesis (82). Increased levels of TNF-α, both systemically in serum and locally in bone, is a key characteristic in several models of inflammatory-mediated bone loss (52, 56), including inflammatory bowel disease (IBD), type 2 diabetes, osteoporosis, and exposure to space-relevant radiation (1).

1.2.3. Mitigating Radiation-Induced Bone Loss

As human exploration of space continues to expand and humans seek to travel further into deep space, the need for a countermeasure to protect against the negative impact of radiation exposure on bone integrity is paramount. Physical countermeasures against skeletal unloading have already been employed in space, as well as use of anti-bone resorption medications (58, 60). Much of the literature on this topic focuses on pharmacological, anti-oxidant, and nutritional countermeasures to radiation-induced bone loss. Pharmacological agents, particularly the bisphosphonate class of drug, appears to be moderately effective to prevent the loss of bone, particularly when combined with exercise (60). Likewise, anti-oxidants, specifically alpha-lipolic acid and dried plum supplementation, have been documented to reduce detrimental impacts of radiation on bone (53, 96). However, with upcoming missions exceeding one year in space, the need for further identification of countermeasures to protect against radiation exposure is a major priority to maintain astronaut health.

1.2.3.1. Omega-3 Fatty Acids: Dietary Modulation of Inflammation

One hallmark of the western diet is a large ratio of omega-6 to omega-3 fatty acids, meaning that omega 6 fatty acid intake outweighs that of omega-3 fatty acids (100, 102). Alongside a rise in fat composition of diets, dietary consumption omega-6:omega-3 fatty acids have risen from 0.79:1 in the Paleolithic Era to a ratio of 16.74:1 in the United States (100, 102). Omega-6 and omega-3 fatty acids exert differential effects on body fat gain via altered lipid metabolism, storage, and regulation and inflammation signaling (102). An increase in the omega-6:omega-3 ratio is highly proinflammatory and contributes to the prevalence of diseases such as obesity and diabetes (26, 54, 100–102). Conversely, consumption of a diet rich in omega-3 fatty acids is associated with a low incidence of these diseases and improved health outcomes in inflammation-related chronic diseases, like cancer, rheumatoid arthritis, and inflammatory bowel disease (54, 79, 85, 102, 118).

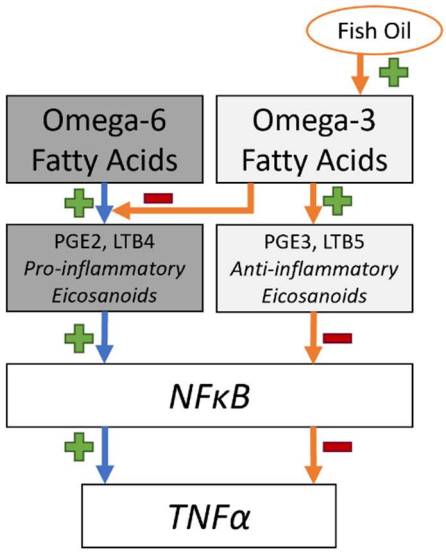

Figure 1-5. Omega-3 vs. Omega-6 mechanism of action to modulate inflammation.

Omega-3 fatty acids are associated with increased cancellous bone mineral density in elderly humans (80, 119) and in C57Bl/6 mice (8). Animals models using ovariectomies have found fish oil, a rich source of omega-3 fatty acids, can prevent post-menopausal bone loss compared to animals fed corn oil, specifically by attenuating loss of BV/TV and Tb.N (7, 81, 93, 108). Further, astronauts consuming an omega-3 fatty acid rich diet experienced attenuated reductions in bone mineral density due to skeletal unloading over 6-month missions on the International Space Station (133).

A potential mechanism to explain these mitigations in bone loss is the reduction in circulating pro-inflammatory markers (99). Omega-3 fatty acids are heavily linked to a class of key inflammatory mediators called eicosanoids (113). Eicosanoids regulate both the intensity and duration of an inflammatory response (50, 113). Inflammatory cells, specifically neutrophils, monocytes, and macrophages, produce TNF-α, via LBT_4 (113). Consumption of omega-3 fatty acids reduces production of LBT_4 and thus other inflammatory cytokines (49, 62). Omega-3 fatty acids also mediate inflammatory gene expression (16, 17). Most notably, nuclear factor kappa B (NF-κB), a transcription factor upstream of TNF-α, is blocked by eicosapentaenoic acid, the eicosanoid derived from omega-3 fatty acids (68, 86, 132). The mechanism of action is depicted in Figure 1-5. Nakanishi *et al*. showed a 5% fish oil diet decreased osteoclast number and activity and suppressed gene expression of NFκB, RANKL, TNFα, IL-6, and PGE2, a downstream target of omega-6 fatty acids and a pro-inflammatory eicosanoid, compared to 5% corn oil, similar to diets used in S1 (81).

1.3. Diet-Induced Inflammation

1.3.1. Diet-Induced Obesity

In the United States, ~40% adults and ~20% of children are classified as obese (39). Obesity in humans, though a complex genetic picture, is strongly associated with overfeeding and poor nutrition (92). The average US citizen's diet is composed of ~48.5% carbohydrate, ~15.5% protein and ~33% fat, with ~10% of total calories coming from fructose (20, 77). Consumption of a high fat, high sugar diet is one factor which predisposes children to obesity, alongside physical inactivity among others (25). The literature surrounding the impact of high fat feeding on skeletal biology is extensive, though no studies have examined the impact of overfeeding via a high fat and high sugar diet, despite research showing both high fat and fructose-rich diets independently exert a negative impact on skeletal biology (32, 105, 106). It is important to note the primary limitation to research surrounding the impact of a high fat diet on bone is the failure to utilize a model of overfeeding, another hallmark of diet-induced obesity, as well as failure to effectively model diet through both high fat composition, high sugar composition, fat source, and addition of sugar-sweetened beverages.

1.3.1.1. High Fat Feeding

High fat feeding, utilizing a diet of 45 or 60% fat, is strongly associated with infiltration of fat in the bone marrow niche and is often accompanied by detriments to bone quality and bone strength, specifically decreases in cancellous bone volume (BV/TV) and trabecular thickness (Tb.Th) and increases in trabecular separation (Tb.Sp), as well as decreased cortical thickness (Ct.Th) and increased cortical porosity

(69, 72, 105, 111). Lu *et al*. fed 2.5-week-old male C57Bl/6 mice a 45% fat diet for eight weeks and showed lower mechanical strength, specifically peak load and stiffness, with corresponding lower relative total, trabecular, and cortical BMD of the tibia (69). High fat fed mice had fewer available osteoblast progenitor cells and exhibited decreased expression of osteogenic genes β-catenin and RUNX2 and increased expression of adipogenic genes PPARγ and aP2 compared to mice fed a normal chow diet (69). Similarly, consumption of a 60% fat diet in 8-week-old male C57Bl/6 mice for 12 weeks led to decreased trabecular bone mass and trabecular number and increased trabecular separation, decreased cortical bone volume and cortical thickness, and increased marrow adiposity (111). Conversely, 12-weeks of exposure to a 60% fat diet in 3-week-old male C57Bl/6 mice led to a significant increase in marrow adiposity, but no change in bone parameters (27). The degree to which a high fat diet negatively impacts skeletal parameters appears to be dependent on several factors, including sex, age at diet onset, duration of diet, rodent strain, diet composition, and physical activity levels, among others.

Despite significant weight gain in rodents fed a high fat diet, there appears to be no positive impact of increased mechanical stimulation on bone growth, specifically bone formation and marrow apposition rates, bone mass or bone strength (36, 69, 89, 94, 98, 131). Exercise has been repeatedly shown to be protective against the impact of high fat feeding on bone parameters, with sedentary rodents showing exacerbated detriments (72, 105). Voluntary wheel running in mice has been shown to eliminate the increase in marrow adipose tissue (MAT) and maintain bone mass in both cancellous and cortical

bone despite consumption of a high fat diet (72, 105). Together, these data suggest the mechanical stimulus for bone growth may be *insufficient* to overcome the negative impact of diet-induced obesity (89, 94, 98, 131).

1.3.1.2. Fructose-Rich Diets

To date, few studies have evaluated the impact of a fructose-rich diet on bone biology, with conflicting reports. Felice *et al*. found a moderately negative impact utilizing a standard chow diet with excess calories supplied in the form of 10% fructose solution in place of regular drinking water (32). In addition to the development of metabolic syndrome, rats fed a fructose-rich diet showed significant increases in marrow adiposity, decreased osteocyte density in cancellous bone, and evidence for an increased adipogenic capacity of mesenchymal stem cell progenitors. The average US citizen consumes a diet that is far higher in fat content, as well as in total calories from fructose, than what is modeled in this study; however, given that moderate decrements are still shown, this provides strong evidence for the negative impact of fructose-rich diets. Conversely, Yarrow *et al.* utilized an *isocaloric* model to compare the addition of 40% fructose to a 30% fat diet for 12 weeks, with fructose supplied as the carbohydrate source (128). Mice fed with 30% fat, regardless of fructose, had significant increases in fat mass and decreases in fat mass, despite no difference in total body weight. Cancellous bone parameters, specifically bone volume fracture, trabecular number and trabecular separation, were negatively impacted and marrow adiposity increased significantly, though cortical bone showed an increased thickness in response to high fat feeding, independent of fructose intake. The authors concluded no additional impact of

fructose on bone, in the context of a high fat diet, however, this study does not utilize a model of overfeeding nor does it assess the impact of fructose in the form of sugar-sweetened beverages, thus limiting the applicability of the results to the average US citizen. Similarly, Tian *et al.* fed C57Bl/6 mice a standard chow (13% fat, 65% carbohydrate), high fructose diet (HFrD; 13% fat, 69% carbohydrate), or a high fat diet (HFD; 60% fat, 20% carbohydrate) for 8, 16 or 24 weeks (112). HFrD mice had higher femoral trabecular bone mass vs. chow-fed mice at all time points, with bone mass peaking in HFrD mice at 16 weeks. HFD mice had higher bone mass vs. chow-fed mice at 8 weeks, with lower bone mass at 16 and 24 weeks. HF feeding led to higher epidydimal fat mass accumulation than HFr feeding. RUNX2, a key transcription factor for osteoblast differentiation, mRNA expression was higher in both HFrD and HFD mice at 8 and 16 weeks, but decreased by 24 weeks. These data suggest that these diets have a positive short-term impact on bone, but long-term consumption results in bone loss.

1.3.2. Mechanisms of Action

Diet is a key contributor to the maintenance of gut integrity. A poor diet can lead to leaky gut syndrome, whereby a microbe imbalance causes separation of colonocytes allowing for harmful bacteria to pass through (64, 65). This increase in intestinal permeability results in an inflammatory response and increased production of inflammatory cytokines. Conversely, consumption of a healthy diet allows for the maintenance of gut integrity and does not exacerbate levels of inflammatory cytokines. Inflammatory cytokines produced at the gut, like TNFα, diffuse into the blood and lead

to high levels of systemic inflammation, which is strongly associated with bone loss (52, 56, 64, 65, 82, 90).

Gut microbiota play a major role in the maintenance of bone mass (72, 103, 120, 127). This was first discovered by Sjorgen *et al.* in germ-free (GF) mice (103). GF mice have higher bone volume fraction (BV/TV) and trabecular number (Tb.N) and lower trabecular separation (Tb.Sp) compared to conventionally raise mice. Further, when GF mice are re-introduced to microbes, bone mass decreases to the level of conventionally raised mice. Mechanistically, gut microbiota exert a robust influence on immune cells critical for bone homeostasis (47). GF mice have low immune cell activation and higher levels of insulin-like growth factor 1 (IGF-1), both of which promote an increase in bone mass (47, 127).

Gut microbiota are largely determined by diet composition (38, 47). Consumption of a high fat diet significantly alters microbial composition and lowers diversity, termed dysbiosis (47, 55). Interestingly, gut microbiota are altered in obese individuals relative to lean individuals, even on the same diet, elucidating a specific role of obesity in microbial composition (114). Intestinal dysbiosis promotes increases in inflammation via toll-like receptor 4 and downstream activation of TNFα (55, 120). In addition to increased inflammation, consumption of a high fat diet leads to increased adipogenesis via increased activation of PPARγ and decreased differentiation of osteoblasts via decreased expression of β-catenin and RUNX2 (69). Prolonged alterations in the microbiome and consumption of a western diet, particularly during skeletal development, lead to detriments to bone quality and strength (74).

1.3.3. Mitigating Bone Loss in Diet-Induced Obesity

To date, only one study has evaluated the impact of diet alterations following high fat feeding on bone quality. Scheller *et al.* fed 6-week-old male C57Bl/6 mice a 60% HF diet or a 13.5% normal chow diet (95). After 12 weeks, one group on the HF diet were switched to the normal chow diet for 8 weeks. HF feeding led to increased marrow adiposity and significant detriments to cortical and cancellous microarchitecture compared to a normal chow diet. Mice switched from the HF diet had attenuated expansion of marrow adiposity and partially rescued bone microarchitecture, supporting a major role for diet alterations in rescuing bone quality in diet-induced obesity.

Diet supplementation using pre- or pro-biotics have been successfully employed to improve bone outcomes (64, 71). Certain pro-biotics are capable of inhibiting differentiation of osteoclasts, promoting osteogenic markers and absorption of calcium into bone, and reducing expression of inflammatory markers (65). Supplementation with beneficial microbes can moderately increase bone mineral density (BMD) and can even prevent bone loss caused by sex-steroid deficiency (64). For example, insertion of *L. reuteri* directly into the gut of mice, termed oral gavage, tri-weekly for 4 weeks led to increased bone volume, bone mineral density, trabecular number and trabecular thickness and decreased trabecular spacing via increases in serum osteocalcin, a protein secreted by osteoblasts to promote calcium storage in bone, and bone formation rates (71). Interestingly, this effect was noted in male, but not female, mice. *L. reuteri* acts to promote bone formation via suppression of TNFα transcription (64). McCabe *et al.* hypothesized that female mice showed no effect due to saturation of the pathway via

estrogen signaling (71). In conjunction with the work of Sjorgen *et al*. in GF mice and studies utilizing pro- and pre-biotic supplementation, these provide evidence for a positive impact of supplementation of beneficial microbes via fecal microbial transplants (FMT) on bone health.

1.4. Purpose & Study Aims

Two independent studies were completed to investigate the mechanisms surrounding inflammation-mediated bone loss. The purpose of Study 1 (S1) was to determine if dietary modulation of inflammatory cytokines can mitigate radiation-induced bone loss via reductions in local and systemic inflammation. The purpose of Study 2 (S2) was to determine if alterations in diet, with and without supplementation of microbiota from healthy mice, can rescue bone quality. These aims seek to explore the ability for an anti-inflammatory diet to reduce inflammation-mediated damage to bone and the ability for diet and microbiota supplementation to reverse the negative effects of a pro-inflammatory diet on bone, in S1 and S2, respectively. The sections below detail the methodologies that have been and will be performed across both studies.

2. DIETARY MODULATION OFI NFLAMMATORY CYTOKINES IN RADIATION-INDUCED BONE LOSS

The purpose of Study 1 (S1) was to determine if dietary modulation of inflammatory cytokines can mitigate radiation-induced bone loss by reducing inflammation locally in bone and systemically in serum. This aims seek to explore the ability for an anti-inflammatory diet to reduce inflammation-mediated damage applied via irradiation to bone. We hypothesized that consumption of a diet high in omega-3 fatty acids can mitigate negative impacts to bone biology via reductions in both local and systemic inflammation. The sections below detail the methodologies that have been and will be performed across both studies.

2.1. Methods

Adult (30- to 50-week old) female Lgr5-EGFP C57BL/6 mice (n=4-6/group) were randomly assigned to corn oil and cellulose (COC) or fish oil and pectin (FOP) diets. Mice were acclimated to assigned diets for three weeks prior to radiation exposure and remained on assigned diets for the duration of the study (Figure 2-1). Animals were

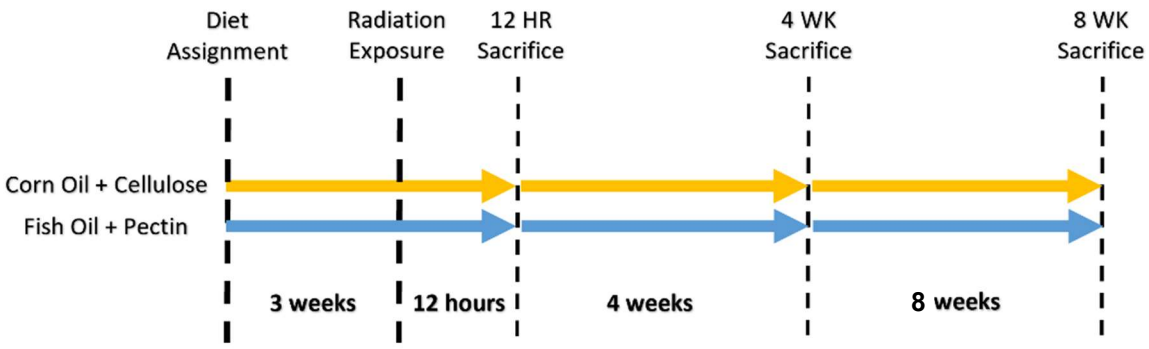

Figure 2-1. S1 Experimental Timeline

block assigned to radiation groups to achieve balanced age and body weights across COC and FOP groups and within all doses of ^{56}Fe and gamma radiation. Animals were terminated 12 hours, 4 weeks and 8 weeks after irradiation and tissues were collected for analysis.

2.1.1. Animals

A breeder colony of Lgf5-EGFP-IRES-cre ER^{T2} knock-in transgenic mice utilizing a C57BL/6 background was established with founder heterogeneous males and wild type females. Breeder colony mice were maintained on 9% or 4% protein custom-designed diets for breeders or maintenance, respectively. Mice were weaned and separated by sex at 21 days of age and genotype status was determined via tail snip DNA. Transgenic mice were maintained on a 4% protein diet until study onset. Stem cells of intestinal and colon cells fluoresce in Lgr5-EGFP C57BL/6 mice, which was required for the specific aims of the parent study. According to the Protein Atlas database, bone has no known gene or protein expression of Lgr5 (116). Though no study has looked into the potential side effects on bone, control Lgr5-EGFP C57Bl/6 mice in our study have a bone phenotype consistent with female, aged-matched wildtype C57Bl/6 mice (44). Wildtype C57BL/6 mice have been extensively used to study the impact of radiation exposure on bone as a model for radiation-induced bone loss in humans (41). The majority of radiation-induced bone loss investigate the impact in male mice (1, 2, 53, 121, 129). As the number of female astronauts grows, it is imperative to assess the expected biological impact of radiation to bone, thus female mice were utilized in this study.

This study was approved and followed procedures set by the Texas A&M Institutional Animal Care and Use Committee. All animals were housed individually housed after group assignment in the university vivarium with 12-h light/dark cycles.

2.1.2. Diet

Animals were randomly assigned to an *ad libitum* diet: a corn oil and cellulose (COC) diet consisting of 6% cellulose and 5% corn oil or a fish oil and pectin (FOP) diet consisting of 6% pectin, 4% fish oil and 1% corn oil, with all other ingredients maintained across diets (Table 1). The COC diet is used to mimic a diet high in omega

Ingredient	COC	FOP
Sucrose	42.00%	42.00%
Casein	20.00%	20.00%
Corn Starch	22.00%	22.00%
Pectin	0.00%	6.00%
Cellulose	6.00%	0.00%
AIN-76A Salt Mix	3.50%	3.50%
AIN-76A Vitamin Mix	1.00%	1.00%
DL-Methionine	0.30%	0.30%
Choline Chloride	0.20%	0.20%
Fish Oil	0.00%	4.00%
Corn Oil	5.00%	1.00%

Table 2-1. Comparison of experimental diets composition (percent of weight). Diets differ in fiber and lipid sources.

-6 fatty acids, while the FOP diet is rich in omega-3 fatty acids. A high omega-6:omega-3 ratio is highly pro-inflammatory and may lead to systemic chronic inflammatory responses. Conversely, consumption of a diet rich in omega-3 fatty acids is highly anti-inflammatory and has been documented to reduce systemic inflammation (118). Further, high consumption of omega-3 fatty acids has been demonstrated to attenuate reductions

in bone mineral density in astronauts due primarily to skeletal unloading over 6-month missions on the International Space Station (133), thus demonstrating a potential role for omega-3 fatty acids to mitigate bone loss.

2.1.3. Radiation Exposure

Animals were randomized to receive exposures to total body low dose high-energy radiation (0.1, 0.25, 0.5 Gy of 1000 MeV/n ^{56}Fe at 25 cGy/min at Brookhaven National Lab), to an equivalent dose of gamma radiation (0.2, 1.1, 2.0 Gy of γ at 25 cGy/min at TAMU Nuclear Science Center), or non-irradiated controls (sham). Sham animals were treated identically to irradiated animals aside from combined anesthesia and radiation exposure. Mice exposed to ^{56}Fe radiation were shipped from Texas A&M University to Brookhaven National Laboratory (Upton, NY) and acclimated for 1 week prior to radiation exposure. Animals were terminated at 12 hours, 4 weeks and 8 weeks post-radiation exposure. Animals assigned to terminations at 4- and 8-weeks post-exposure to ^{56}Fe radiation were shipped to Texas A&M University at least 4 days after irradiation to prevent excessive stress to the animal. Mice assigned to gamma radiation were irradiated at Texas A&M University.

2.1.4. Euthanasia & Tissue Collection

Animals were euthanized using carbon dioxide or 3-4% isoflurane inhalation followed by cervical dislocation. Blood was collected via cardiac puncture after thoracotomy. Left and right femora and tibiae were collected and stored appropriately for analyses, as described below.

2.1.5. Serum Analysis of TNFα

Immediately following collection at termination, whole blood was centrifuged at 4°C at 1500g for 15 minutes and serum was separated and stored at -80°C until analysis. Serum TNFα was measured in a quantitative immunoassay ELISA (R&D Systems, Minneapolis, MN, USA) for all time points. Calculation of results was carried out according to manufacturer's guidelines. Serum TNFα was assessed across all termination timepoints.

2.1.6. Micro-computed Tomography

Micro-computed tomography (μCT) was performed at the distal metaphysis and mid-diaphysis of the right femur using a high-resolution imaging system (μCT 50, ScanCo, Bruttisellen, Switzerland) to assess bone geometry and microarchitecture. Left femora were fixed in 4% phosphate-buffered formalin and subsequently stored in 70% ethanol at 4°C until immediately prior to scanning. Distal and mid-diaphyseal femoral regions were scanned at 9 μm isotropic voxel size using 55 kVp, 114 mA, and 200-ms. Cancellous bone parameters analyzed include bone volume fraction (BV/TV; %), trabecular thickness (Tb.Th; mm), trabecular number (Tb.N; mm^{-1}), trabecular separation (Tb.Sp; mm), connective density (Conn.D; mm^{-3}), and volumetric bone mineral density (vBMD; g/cm^3). Analysis of cancellous bone regions was performed using a semi-automated contouring program that separated cancellous from cortical bone. Cortical bone was assessed in a 1-mm-long region centered at the mid-diaphysis. Cortical bone parameters analyzed include cortical area (Ct.Ar; mm^2), cortical thickness (Ct.Th; mm), total area (T.Ar; mm^2), medullary area (Med.Ar; mm^2), periosteal diameter

(Peri.Dm; mm), and endocortical diameter (Endo.Dm; mm). Bone was segmented from soft tissue using the same threshold for all groups: 245 mg HA/cm^3 for cancellous and 682 mg HA/cm^3 for cortical bone. All scan acquisition and analyses described here are in agreement with established guidelines for use of μCT in rodents (12).

2.1.7. Immunohistochemical Staining of Osteocytes Positive for Proteins of Interest

Left femora were collected from animals at termination, fixed in 4% phosphate-buffered formalin for 24 hours and subsequently stored in 70% ethanol at 4°C. Bones were then decalcified in a sodium citrate/formic acid solution for approximately 12 days prior to dehydration and processing using a Thermo-Scientific STP 120 Spin Tissue Processor and were paraffinized via a Thermo Shandon Histocenter 3 Embedding tool. Longitudinal sections of the femur were cut on a Leica microtome (RM2125, Leica, Wetzlar, Germany) to approximately 5 μm thickness, mounted on positively charged slides, and baked overnight at 37°C. Slides were later stained for proteins of interest using an avidin-biotin method. Briefly, heat-mediated antigen retrieval was performed when specified by manufacturer instructions using 1% triton in phosphate-buffered saline. Samples were rehydrated, peroxidase inactivated using 3% H_2O_2/methanol, permeabilized using 0.5% Triton-X 100 in phosphate-buffered saline, blocked with species-appropriate serum for 30 minutes at room temperature (Vectastain Elite ABC; Vector Laboratories, California, USA) and incubated overnight at 4°C with primary antibodies: polyclonal rabbit anti-TNFα (1:200; Abcam, Cambridge, UK), polyclonal goat anti-Sclerostin (1:150; R&D Systems, Minnesota, USA), and polyclonal rabbit anti-IGF-1 (1:200; R&D Systems, Minnesota, USA). Sections were incubated at room

temperature for 45 minutes with species-appropriate biotinylated anti-IgG secondary antibody. Peroxidase development was performed with an enzyme substrate kit (diaminobenzidine [DAB]; Vector Laboratories, California, USA). Counterstaining was conducted with methyl green counterstain (Vector Laboratories, California, USA) for 2.5 minutes. Sections were then dehydrated into organic phase and mounted with xylene-based mounting media (Polysciences, Pennsylvania, USA). Negative controls for all antibodies were completed by omitting only the primary antibody. Quantification of immunohistochemical analyses were performed using OsteoMeasure Analysis System, version 3.3 (OsteoMetrics, Inc., Georgia, USA) interfaced with a light microscope and CCD camera (DP73, Olympus, Tokyo, Japan). The proportion of all osteocytes stained positively for the protein of interest was quantified in cancellous bone, starting ~500 μm from the growth plate within an area of ~4 mm^2, and in cortical bone at mid-diaphysis, within an area of ~1 mm^2 per side, at a magnification of 400x (Figure 2-2).

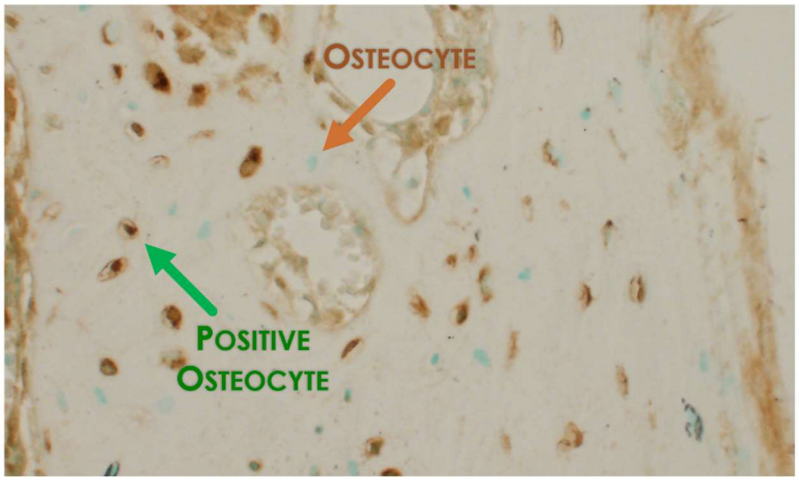

Figure 2-2. Immunostaining for protein of interest depicting an osteocyte vs. an osteocyte positive for the protein of interest. Image taken at magnification of 400x.

2.1.8. Marrow Adipocyte Quantification

Left femora were collected, decalcified, paraffinized and sectioned as described in the preceding section. Slides were subsequently treated with hematoxylin counterstain (Vector Laboratories, California, USA) to measure adipocyte volume/total volume (AV/TV, %), adipocyte number (#/mm), and average adipocyte size (μm^2). Briefly, slides were rehydrated, counterstained with hematoxylin for 30 seconds, rehydrated and mounted using xylene-based mounting media (Polysciences, Pennsylvania, USA). Histomorphometric analyses were performed using OsteoMeasure Analysis System, version 3.3 (OsteoMetrics, Inc., Georgia, USA) interfaced with a light microscope and CCD camera (DP73, Olympus, Tokyo, Japan). A defined region of interest was established, starting ~500 μm from the growth plate within an area of ~4 mm^2 at a magnification of 200x. Adipocytes were visually identified and quantified manually as previously described (88) (Figure 2-3).

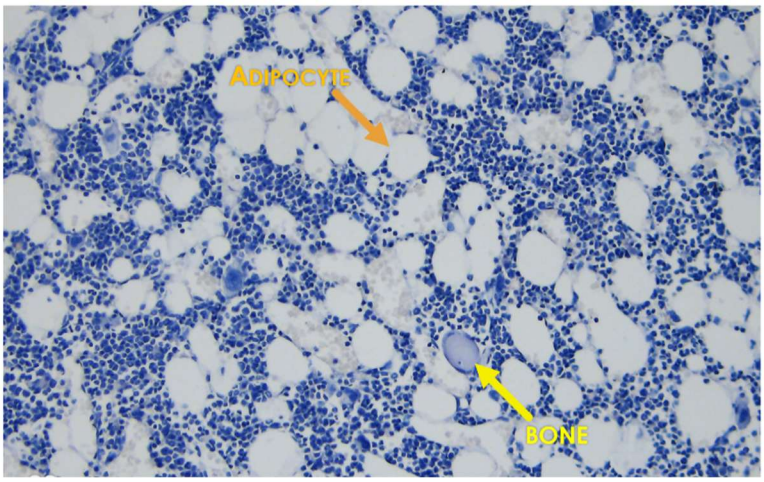

Figure 2-3. Histological staining using hematoxylin to visually identify marrow adipocytes at the distal femoral metaphysis. Image taken at 200x.

2.1.9. Static Histomorphometry

Static histomorphometry was performed at the distal femoral metaphysis to assess relative osteoid and osteoclast surfaces. Distal right femora were fixed in 4% phosphate-buffered formalin for 24 hours and subsequently stored in 70% ethanol at 4°C. Femora were then subjected to serial dehydration and embedded in methyl methacrylate (Sigma-Aldrich, Missouri, USA). Samples were sectioned on a Leica microtome (RM 2255, Leica, Wetzlar, Germany) to approximately 5 µm thickness, mounted on gelatinized slides and baked for ~48 hours at 37°C. Slides were subsequently treated with von Kossa stain and tetrachrome counterstain to measure osteoid (OS/BS, %) and osteoclast surfaces (OcS/BS, %), relative to total cancellous surface. Histomorphometric analyses were performed using OsteoMeasure Analysis System, version 3.3 (OsteoMetrics, Inc., Georgia, USA) interfaced with a light microscope and CCD camera (DP73, Olympus, Tokyo, Japan). A defined region of interest was established, starting beginning ~500 µm from the growth plate and within an area of ~4 mm^2 at a magnification of 400x. Osteoid and osteoclast-covered surfaces were visually identified and quantified manually. (Figure 2-4).

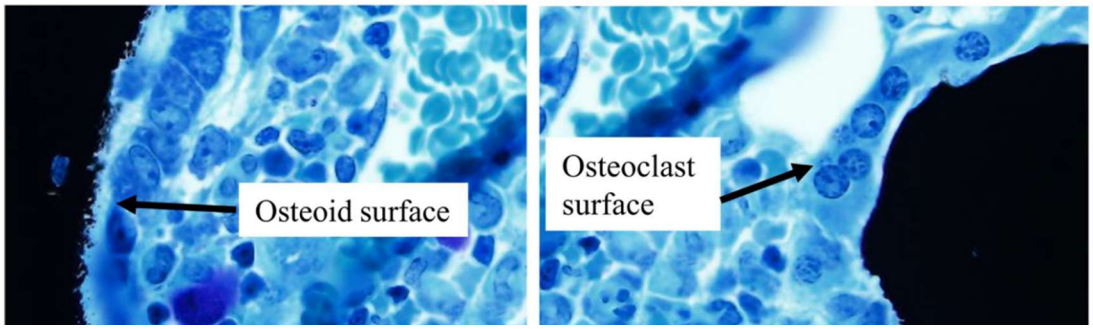

Figure 2-4. Histological staining using von Kossa and tetrachrome counter stain to visually identify osteoid surface and osteoclast surface relative to bone surface.

2.1.10. Statistical Approach

Statistical analyses were performed on all outcome measures using a two-way ANOVA (factors = diet, dose) with each time point and ion species analyzed separately. Data was assessed for normality and outliers, defined as any value greater than 2.5 standard deviations above the mean. An alpha level of 0.10 was set *a priori* to achieve sufficient power (β=0.80) with an *n* of 4-6 per group.

2.2. Results

2.2.1. Serum Analysis of TNFα

Gamma: A significant interaction of *diet x dose* was found for serum concentration of TNFα in mice exposed to γ radiation at 12 hours (p=0.078), such that FOP-fed mice had higher serum TNFα at the highest doses of radiation exposure (Figure 2-5A). A significant main effect of *diet* (p=0.024) was found at 4 weeks. At 8 weeks, there were significant main effects of *diet* (p=0.001) and *dose* (p=0.009). FOP-fed mice had higher serum TNFα compared to COC-fed mice at all doses except 1.1 Gy and serum TNFα levels generally decrease as exposure increases. In COC-fed mice, serum TNFα levels increase modestly with increasing dose of γ radiation.

Iron: A significant interaction of *diet x dose* was found in serum concentration of TNFα in those mice exposed to ^{56}Fe radiation at 12 hours (p<0.001), 4 weeks (p=0.010), and 8 weeks (p=0.007) (Figure 2-5B). At 12 hours, FOP-fed mice had lower serum TNFα at higher doses of ^{56}Fe exposure, in contrast to the impact of γ radiation. At 4

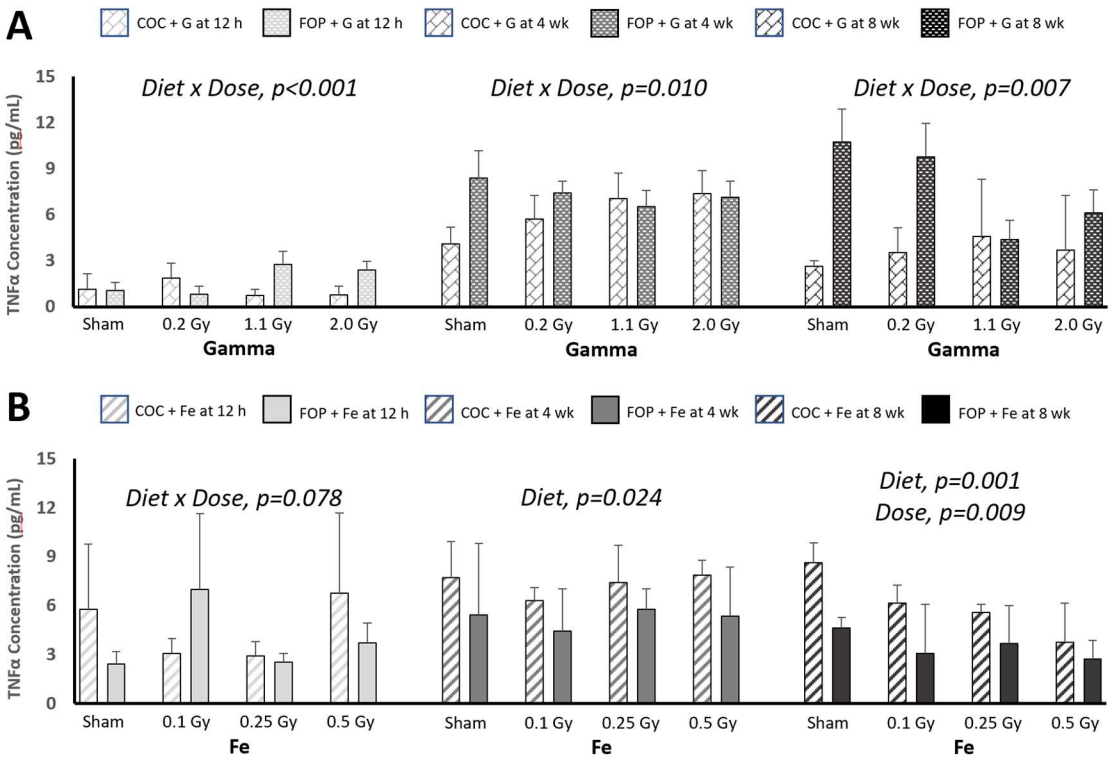

Figure 2-5. Serum TNFα concentrations (pg/mL) 12 hours, 4 weeks, and 8 weeks post-exposure to 3 doses of γ (A) and ^{56}Fe (B) radiation.

weeks, FOP-fed mice had lower serum TNFα at all doses compared to COC-fed mice. At 8 weeks, FOP-fed mice had lower serum TNFα compared to COC-fed mice at all doses; serum TNFα levels in COC-fed mice drop as ^{56}Fe exposure increase.

In the γ cohort, COC-fed mice had generally lower levels of serum TNFα, which were increased with radiation, while FOP-fed mice generally had higher levels of serum TNFα, which were decreased with radiation. In the ^{56}Fe cohort, COC-fed mice had generally higher levels of serum TNFα with a latent effect of lower levels with radiation exposure at 8 weeks.

2.2.2. Micro-computed Tomography Assessment of Bone Geometry & Microarchitecture

Gamma: Four weeks after exposure to γ radiation, no significant effects were detected in BV/TV, Tb.N, Tb.Th, Tb.Sp or vBMD at the femoral metaphysis (Table 2-2). A significant effect of *diet* was found for Conn.Dens (p=0.083) where FOP-fed mice tended to have lower Conn.Dens than COC-fed mice across radiation dose. No significant effects were detected in T.Ar, Ct.Ar, Med.Ar, Peri.Dm, or Endo.Dm at the femoral diaphysis. A significant *diet x dose* interaction was detected for Ct.Th (p=0.042), such that COC-fed mice exhibited generally increased Ct.Th as radiation dose increased, while FOP-fed mice generally decreased Ct.Th as radiation dose increased. At 8 weeks, no significant effects were detected in Tb.N, Tb.Th, or Tb.Sp. A *diet x dose* interaction was found for BV/TV (p=0.064) and Conn.Dens (p=0.009), where COC-fed mice showed lower values while FOP-fed mice showed higher values as dose increased. It's important to note that values for BV/TV and Conn.Dens are lower in FOP-fed sham mice relative to COC-fed shams. A significant effect of *dose* was found for vBMD (p=0.002), where vBMD was generally lower as radiation dose increased. No significant effects were detected for T.Ar at the diaphysis. A significant *diet x dose* interaction was found for Ct.Ar (p=0.071) and Ct.Th (p=0.047). Ct.Ar generally increased in FOP-fed mice as γ radiation dose increased, while COC-fed mice exhibited decreased Ct.Ar at all radiation doses. Despite the opposite effect of *diet* and radiation on Ct.Th at 4 weeks, Ct.Th was maintained at higher radiation doses in FOP-fed mice and reduced at all radiation doses in COC-fed mice. A significant effect of *dose* was detected for Peri.Dm

Table 2-2. Micro-computed tomography of cancellous bone at the distal femoral metaphysis and cortical bone at the femoral diaphysis at 4- and 8-weeks post-exposure to γ radiation.

	Gamma								ANOVA		
	Sham COC	Sham FOP	0.2 Gy COC	0.2 Gy FOP	1.1 Gy COC	1.1 Gy FOP	2.0 Gy COC	2.0 Gy FOP	Diet	Dose	Diet x Dose
Metaphyseal Cancellous											
BV/TV (%)											
4 weeks	4.17 ± 3.19	7.25 ± 4.79	4.75 ± 2.50	3.75 ± 0.96	5.00 ± 2.16	2.25 ± 1.50	4.00 ± 1.41	4.50 ± 1.29	--	--	--
8 weeks	5.75 ± 1.50	2.75 ± 2.36	2.25 ± 0.50	3.00 ± 1.83	3.50 ± 2.38	2.25 ± 0.50	4.00 ± 2.83	5.33 ± 0.82	--	p=0.066	p=0.064
Tb.N (mm^{-1})											
4 weeks	2.94 ± 0.27	3.27 ± 0.49	3.04 ± 0.13	2.97 ± 0.27	2.88 ± 0.25	2.81 ± 0.12	2.83 ± 0.21	2.85 ± 0.12	--	--	--
8 weeks	3.08 ± 0.18	2.91 ± 0.19	2.90 ± 0.10	3.33 ± 0.47	3.03 ± 0.31	3.14 ± 0.57	3.13 ± 0.38	3.22 ± 0.26	--	--	--
Tb.Th (mm)											
4 weeks	0.04 ± 0.01	0.05 ± 0.01	0.05 ± 0.01	0.05 ± 0.00	0.05 ± 0.00	0.05 ± 0.00	0.06 ± 0.01	0.05 ± 0.01	--	--	--
8 weeks	0.06 ± 0.01	0.05 ± 0.00	0.04 ± 0.01	0.04 ± 0.01	0.04 ± 0.01	0.06 ± 0.01	0.05 ± 0.01	0.05 ± 0.00	--	--	--
Tb.Sp (mm)											
4 weeks	0.35 ± 0.03	0.33 ± 0.05	0.36 ± 0.02	0.35 ± 0.04	0.36 ± 0.03	0.37 ± 0.01	0.38 ± 0.02	0.37 ± 0.01	--	--	--
8 weeks	0.35 ± 0.01	0.37 ± 0.02	0.35 ± 0.01	0.32 ± 0.05	0.35 ± 0.03	0.34 ± 0.04	0.34 ± 0.04	0.34 ± 0.03	--	--	--
ConnDens (mm^3)											
4 weeks	27.75 ± 16.67	25.36 ± 15.28	37.46 ± 12.30	7.80 ± 4.16	26.24 ± 18.65	8.28 ± 7.90	19.58 ± 16.16	29.09 ± 18.53	p=0.083	--	--
8 weeks	32.02 ± 3.99	3.92 ± 2.55	16.67 ± 1.25	9.97 ± 6.22	28.19 ± 16.34	8.40 ± 5.66	16.14 ± 2.83	24.53 ± 14.28	p=0.003	--	p=0.009
vBMD (g/cm3)											
4 weeks	922.7 ± 31.5	947.6 ± 18.1	938.3 ± 51.2	940.9 ± 5.8	943.9 ± 26.9	940.6 ± 9.4	965.1 ± 49.2	934.2 ± 6.1	--	--	--
8 weeks	967.1 ± 13.8	955.1 ± 10.2	889.5 ± 59.5	882.4 ± 41.6	912.1 ± 38.0	965.4 ± 21.9	940.4 ± 19.9	932.8 ± 24.3	--	p=0.002	--
Diaphyseal Cortical											
T.Ar (mm^2)											
4 weeks	0.428 ± 0.03	0.423 ± 0.06	0.422 ± 0.028	0.400 ± 0.01	0.407 ± 0.016	0.409 ± 0.020	0.437 ± 0.035	0.403 ± 0.027	--	--	--
8 weeks	0.424 ± 0.04	0.436 ± 0.03	0.41 ± 0.011	0.408 ± 0.02	0.399 ± 0.013	0.432 ± 0.038	0.392 ± 0.016	0.398 ± 0.045	--	--	--
Ct. Ar (mm^2)											
4 weeks	0.037 ± 0.021	0.045 ± 0.008	0.050 ± 0.025	0.038 ± 0.008	0.051 ± 0.020	0.023 ± 0.014	0.040 ± 0.016	0.044 ± 0.011	--	--	--
8 weeks	0.061 ± 0.024	0.030 ± 0.021	0.021 ± 0.008	0.029 ± 0.015	0.032 ± 0.021	0.020 ± 0.004	0.037 ± 0.021	0.045 ± 0.008	--	p=0.038	p=0.071
Med.Ar (mm^2)											
4 weeks	0.236 ± 0.025	0.237 ± 0.048	0.233 ± 0.029	0.219 ± 0.010	0.214 ± 0.009	0.228 ± 0.031	0.253 ± 0.029	0.220 ± 0.022	--	--	--
8 weeks	0.234 ± 0.022	0.245 ± 0.021	0.227 ± 0.019	0.232 ± 0.019	0.225 ± 0.011	0.250 ± 0.026	0.208 ± 0.017	0.227 ± 0.030	p=0.082	--	--
Ct.Th (mm)											
4 weeks	0.044 ± 0.01	0.054 ± 0.01	0.051 ± 0.006	0.051 ± 0	0.053 ± 0.002	0.045 ± 0.002	0.059 ± 0.014	0.052 ± 0.006	--	--	p=0.042
8 weeks	0.056 ± 0.01	0.051 ± 0	0.04 ± 0.006	0.041 ± 0.01	0.041 ± 0.008	0.055 ± 0.007	0.046 ± 0.003	0.052 ± 0.006	--	p=0.005	p=0.047
Peri.Dm. (mm)											
4 weeks	0.683 ± 0.03	0.701 ± 0.04	0.686 ± 0.040	0.698 ± 0.01	0.706 ± 0.028	0.697 ± 0.028	0.745 ± 0.032	0.708 ± 0.040	--	--	--
8 weeks	0.720 ± 0.02	0.714 ± 0.04	0.692 ± 0.011	0.688 ± 0.02	0.662 ± 0.033	0.707 ± 0.017	0.668 ± 0.032	0.665 ± 0.020	--	p=0.007	--
Endo.Dm (mm)											
4 weeks	0.477 ± 0.020	0.492 ± 0.044	0.475 ± 0.043	0.488 ± 0.012	0.482 ± 0.025	0.497 ± 0.031	0.536 ± 0.034	0.495 ± 0.043	--	--	--
8 weeks	0.499 ± 0.007	0.521 ± 0.012	0.484 ± 0.024	0.486 ± 0.029	0.465 ± 0.021	0.512 ± 0.005	0.467 ± 0.044	0.466 ± 0.021	p=0.031	p=0.007	--

Table 2-3. Micro-computed tomography of cancellous bone at the distal femoral metaphysis and cortical bone at the femoral diaphysis at 4- and 8-weeks post-exposure to ^{56}Fe radiation.

	Fe								ANOVA		
	Sham COC	Sham FOP	0.1 Gy COC	0.1 Gy FOP	0.25 Gy COC	0.25 Gy FOP	0.5 Gy COC	0.5 Gy FOP	Diet	Dose	Diet x Dose
Metaphyseal Cancellous											
BV/TV (%)											
4 weeks	4.67 ± 2.09	6.55 ± 0.75	3.74 ± 0.95	3.69 ± 1.58	7.12 ± 2.41	5.61 ± 1.55	4.14 ± 1.81	4.67 ± 4.07	--	--	--
8 weeks	2.62 ± 1.28	3.49 ± 1.44	4.31 ± 0.49	4.86 ± 1.44	3.11 ± 1.39	4.59 ± 2.70	3.67 ± 3.15	2.56 ± 1.14	--	--	--
Tb.N (mm^{-1})											
4 weeks	2.87 ± 0.15	2.96 ± 0.04	2.92 ± 0.22	2.92 ± 0.12	3.17 ± 0.29	2.96 ± 0.09	2.92 ± 0.10	2.99 ± 0.44	--	--	--
8 weeks	2.90 ± 0.29	2.83 ± 0.13	3.08 ± 0.23	2.88 ± 0.13	2.87 ± 0.14	2.89 ± 0.06	3.06 ± 0.27	3.83 ± 1.18	--	p=0.019	p=0.078
Tb.Th (mm)											
4 weeks	0.05 ± 0.00	0.05 ± 0.01	0.05 ± 0.01	0.05 ± 0.01	0.06 ± 0.00	0.06 ± 0.01	0.05 ± 0.00	0.06 ± 0.01	--	--	--
8 weeks	0.05 ± 0.01	0.04 ± 0.01	0.05 ± 0.01	0.05 ± 0.01	0.06 ± 0.01	0.05 ± 0.00	0.05 ± 0.01	0.06 ± 0.01	--	--	p=0.081
Tb.Sp (mm)											
4 weeks	0.37 ± 0.03	0.35 ± 0.00	0.37 ± 0.02	0.36 ± 0.02	0.34 ± 0.03	0.36 ± 0.01	0.36 ± 0.04	0.37 ± 0.04	--	--	--
8 weeks	0.36 ± 0.03	0.36 ± 0.02	0.34 ± 0.03	0.38 ± 0.02	0.37 ± 0.02	0.37 ± 0.02	0.36 ± 0.04	0.36 ± 0.04	--	--	--
ConnDens (mm^3)											
4 weeks	14.61 ± 8.61	15.27 ± 5.64	18.36 ± 6.96	19.62 ± 6.58	36.34 ± 15.11	21.57 ± 13.36	16.99 ± 8.97	27.33 ± 17.69	--	--	--
8 weeks	4.01 ± 3.10	14.80 ± 4.14	17.55 ± 10.36	16.15 ± 3.60	2.84 ± 0.75	19.50 ± 11.92	13.18 ± 11.58	10.98 ± 8.03	p=0.069	--	--
vBMD (g/cm3)											
4 weeks	956.1 ± 17.8	929.1 ± 40.9	958.2 ± 52.1	968.6 ± 70.9	972.2 ± 41.7	965.0 ± 35.3	948.7 ± 23.5	986.0 ± 25.3	--	--	--
8 weeks	939.6 ± 58.2	891.7 ± 24.7	927.9 ± 46.1	901.9 ± 13.2	972.0 ± 43.0	945.3 ± 13.5	941.8 ± 36.3	958.1 ± 57.9	--	--	--
Diaphyseal Cortical											
T.Ar (mm^2)											
4 weeks	0.369 ± 0.013	0.403 ± 0.020	0.390 ± 0.016	0.378 ± 0.042	0.402 ± 0.019	0.388 ± 0.021	0.406 ± 0.021	0.410 ± 0.033	--	--	--
8 weeks	0.444 ± 0.030	0.420 ± 0.039	0.404 ± 0.027	0.395 ± 0.036	0.422 ± 0.026	0.418 ± 0.013	0.408 ± 0.039	0.413 ± 0.013	--	--	--
Ct. Ar (mm^2)											
4 weeks	0.168 ± 0.008	0.168 ± 0.010	0.179 ± 0.008	0.169 ± 0.019	0.189 ± 0.014	0.181 ± 0.010	0.183 ± 0.010	0.180 ± 0.006	--	p=0.017	--
8 weeks	0.192 ± 0.012	0.181 ± 0.016	0.180 ± 0.020	0.164 ± 0.015	0.190 ± 0.025	0.189 ± 0.005	0.180 ± 0.015	0.187 ± 0.011	--	--	--
Med.Ar (mm^2)											
4 weeks	0.198 ± 0.010	0.232 ± 0.012	0.207 ± 0.020	0.206 ± 0.023	0.210 ± 0.022	0.202 ± 0.012	0.219 ± 0.015	0.225 ± 0.029	--	--	--
8 weeks	0.248 ± 0.018	0.235 ± 0.024	0.219 ± 0.011	0.228 ± 0.023	0.227 ± 0.010	0.225 ± 0.010	0.225 ± 0.034	0.222 ± 0.011	--	--	--
Ct.Th (mm)											
4 weeks	0.201 ± 0.008	0.192 ± 0.009	0.212 ± 0.015	0.202 ± 0.010	0.214 ± 0.011	0.214 ± 0.005	0.207 ± 0.008	0.204 ± 0.009	--	p=0.016	--
8 weeks	0.208 ± 0.005	0.204 ± 0.007	0.208 ± 0.018	0.189 ± 0.009	0.214 ± 0.021	0.215 ± 0.004	0.202 ± 0.021	0.213 ± 0.010	--	--	--
Peri.Dm. (mm)											
4 weeks	0.600 ± 0.027	0.653 ± 0.023	0.589 ± 0.016	0.615 ± 0.047	0.573 ± 0.033	0.549 ± 0.128	0.606 ± 0.029	0.613 ± 0.043	--	--	--
8 weeks	0.637 ± 0.030	0.616 ± 0.022	0.649 ± 0.017	0.732 ± 0.048	0.604 ± 0.016	0.674 ± 0.046	0.519 ± 0.071	0.646 ± 0.038	p<0.001	p<0.001	p=0.010
Endo.Dm (mm)											
4 weeks	0.403 ± 0.029	0.459 ± 0.010	0.388 ± 0.014	0.416 ± 0.037	0.363 ± 0.019	0.352 ± 0.096	0.400 ± 0.021	0.413 ± 0.026	--	p=0.013	--
8 weeks	0.434 ± 0.026	0.421 ± 0.017	0.444 ± 0.017	0.531 ± 0.040	0.402 ± 0.014	0.459 ± 0.035	0.334 ± 0.055	0.438 ± 0.042	p<0.001	p<0.001	p=0.012

(p=0.007) and Endo.Dm (p=0.007) such that Peri.Dm increased and Endo.Dm decreased as radiation dose increased. A significant effect of *diet* was detected for Med.Ar (p=0.082) and Endo.Dm (p=0.031), whereby FOP-fed mice had generally higher Med.Ar and Endo.Dm

Iron: No significant effects were detected in cancellous bone at the metaphysis or in T.Ar, Med.Ar, or Peri.Dm. at the diaphysis at 4 weeks after exposure to ^{56}Fe (Table 2-3). A significant effect of *dose* was found for Ct.Ar (p=0.017), Ct.Th (p=0.016), and Endo.Dm (p=0.013). Ct.Ar and Ct.Th are higher, across diet, as dose increases. Endo.Dm is lower at the low and middle doses of ^{56}Fe. At 8 weeks, no significant interactions or effects were detected in BV/TV, Tb.Sp or Conn.Dens at the metaphysis or in T.Ar or Med.Ar at the diaphysis. However, at 8 weeks post-exposure, a significant interaction of *diet x dose* was found for Tb.N (p=0.078) and Tb.Th (p=0.081) at the metaphysis and Peri.Dm (p=0.010) and Endo.Dm (p=0.012) at the diaphysis. Tb.N and Tb.Th are higher as dose increases in FOP-fed mice, and lower as dose increases in COC-fed mice. Peri.Dm and Endo.Dm are higher as dose increases in FOP-fed mice only. A significant effect of *diet* (p=0.069) was found for Conn.Dens, such that FOP-fed mice had higher Conn.Dens at sham and middle doses of ^{56}Fe than COC-fed mice.

In the γ cohort, COC-fed mice had generally lower BV/TV, Conn.Dens, Ct.Ar, Ct.Th, Med.Ar, and Endo.Dm than FOP-fed mice, which were lower with radiation in COC-fed mice and higher in FOP-fed mice. Interestingly, radiation exposure irrespective of diet led to lower vBMD but higher Peri.Dm and Endo.Dm. In the ^{56}Fe cohort, COC-

fed mice had generally lower Tb.N, Tb.Th, Conn.Dens, Endo Dm. and Peri.Dm than FOP-fed mice, with only FOP-fed mice demonstrating gains with radiation exposure.

2.2.3. Immunohistochemical Staining of Osteocytes Positive for Proteins of Interest

Gamma: No significant interactions or effects were detected for the percentage of osteocytes staining positive for TNFα (%+Ot-TNFα) in cancellous bone at the metaphysis 12 hours post-exposure to γ radiation (Figure 2-6 A-B). A significant interaction of *diet x dose* was detected at 4 weeks (p=0.087) such that FOP-fed mice showed higher %+Ot-TNFα at lower doses of radiation, but a decrease as dose increased. COC-fed mice showed lower %+Ot-TNFα at lower doses of radiation, but an increase as dose increased. In cortical bone at the mid-diaphysis, a significant interaction of *diet x dose* was found at 12 hours (p=0.065) and 4 weeks (p=0.092), with no significant interaction or effects at 8 weeks. At both 12 hours and 4 weeks, %+Ot-TNFα in FOP-fed mice was lower as dose increased and in COC-fed mice %+Ot-TNFα was higher as dose increased.

Iron: No significant interactions or effects were detected in %+Ot-TNFα in cancellous or cortical bone at 4 and 8 weeks with exposure to ^{56}Fe (Figure 2-6 C-D). In cancellous bone at the metaphysis at 12 hours, a significant interaction of *diet x dose* (p=0.081) was found. FOP-fed mice had higher %+Ot-TNFα at lower doses of radiation and lower %+Ot-TNFα at the highest dose. COC-fed mice had lower %+Ot-TNFα at the lowest dose of radiation only. In cortical bone at the mid-diaphysis at 12 hours, there was a significant interaction of *diet x dose* (p=0.016), such that across diets %+Ot-TNFα was higher at lower doses of radiation and decreased as radiation increased. FOP-fed

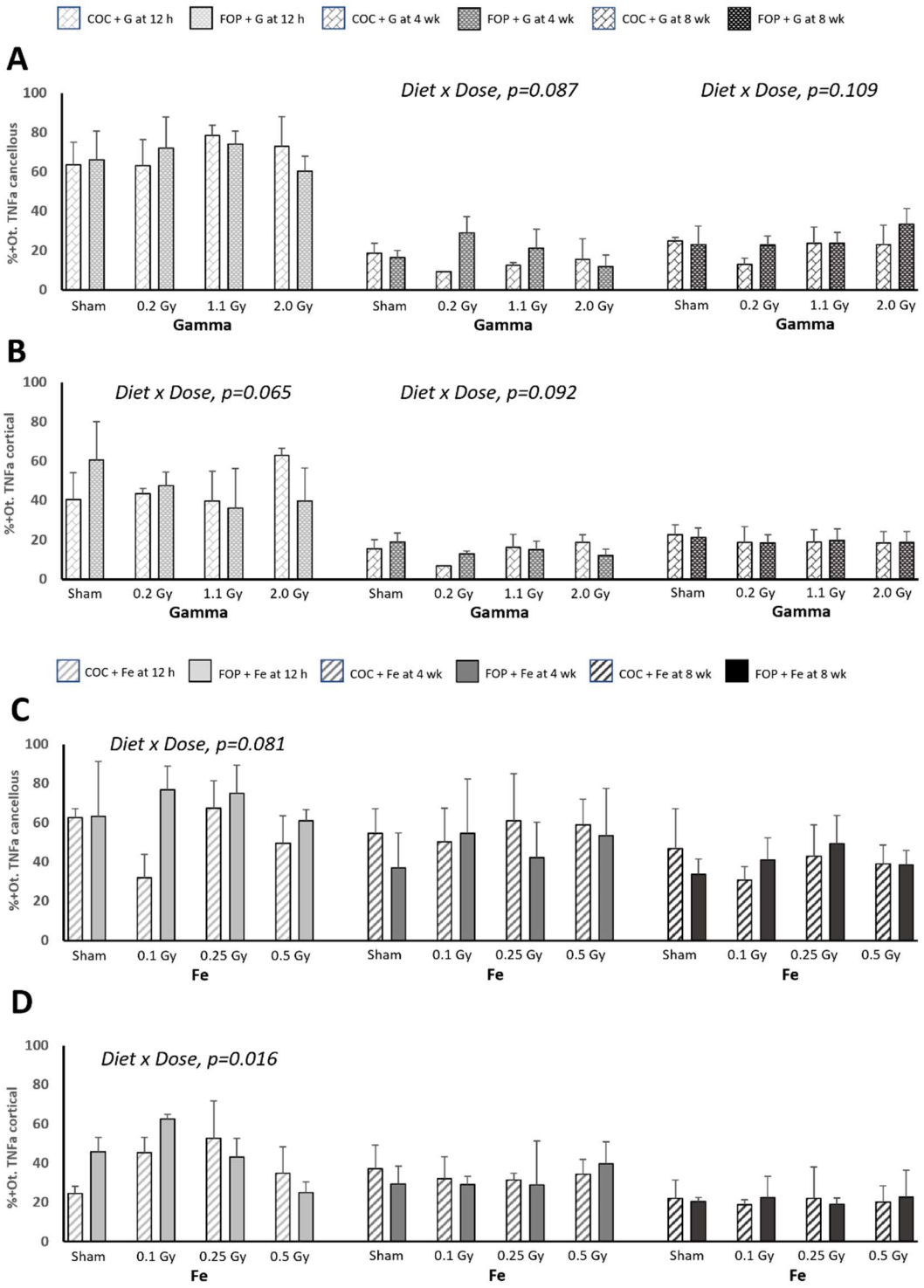

Figure 2-6. Percentage of osteocytes staining positive for TNFα 12 hours, 4 weeks, and 8 weeks post exposure to γ radiation in cancellous (A) and cortical bone (B) and ^{56}Fe in cancellous (C) and cortical bone (D).

mice had higher %+Ot-TNFα with sham and low radiation exposure, but lower at middle and higher doses.

In the γ cohort, COC-fed mice had generally a lower %+Ot-TNFα than FOP-fed mice, which was higher with radiation in cancellous bone. Interestingly, in the ^{56}Fe cohort, minimal differences were detected between groups.

Gamma: No significant interactions were detected at 12 hours or 8 weeks in %+Ot-Scl in cancellous bone or at all time points in cortical bone with γ radiation exposure (Figure 2-7 A-B). At 4 weeks in cancellous bone at the metaphysis, %+Ot-Scl showed a significant effect of *diet* (p=0.082), such that FOP-fed mice had lower %+Ot-Scl with sham and low radiation exposure.

Iron: No significant interactions were detected at all time points in %+Ot-Scl in cancellous bone or at 12 hours of 8 weeks in cortical bone with exposure to ^{56}Fe (Figure 2-7 C-D). At 4 weeks in cortical bone at the mid-diaphysis, %+Ot-Scl showed a significant effect of *dose* (p=0.079), such that across diets %+Ot-Scl was lower as dose increased.

Iron: No significant interactions or effects were detected in %+Ot-IGF-1 in cortical or cancellous bone with exposure to ^{56}Fe at 4 weeks (Figure 2-8 A-B). At 8 weeks, %+Ot-IGF-1 in cancellous bone at the metaphysis revealed significant effects of dose (p=0.067) and diet (p=0.082); FOP-fed mice showed a higher %+Ot-IGF-1 at low and middle doses of ^{56}Fe than COC-fed mice. At 8 weeks, %+Ot-IGF-1 in cortical bone at the mid-diaphysis showed a significant effect of *dose* (p=0.079). Across diets, %+Ot-IGF-1 generally increases with radiation dose.

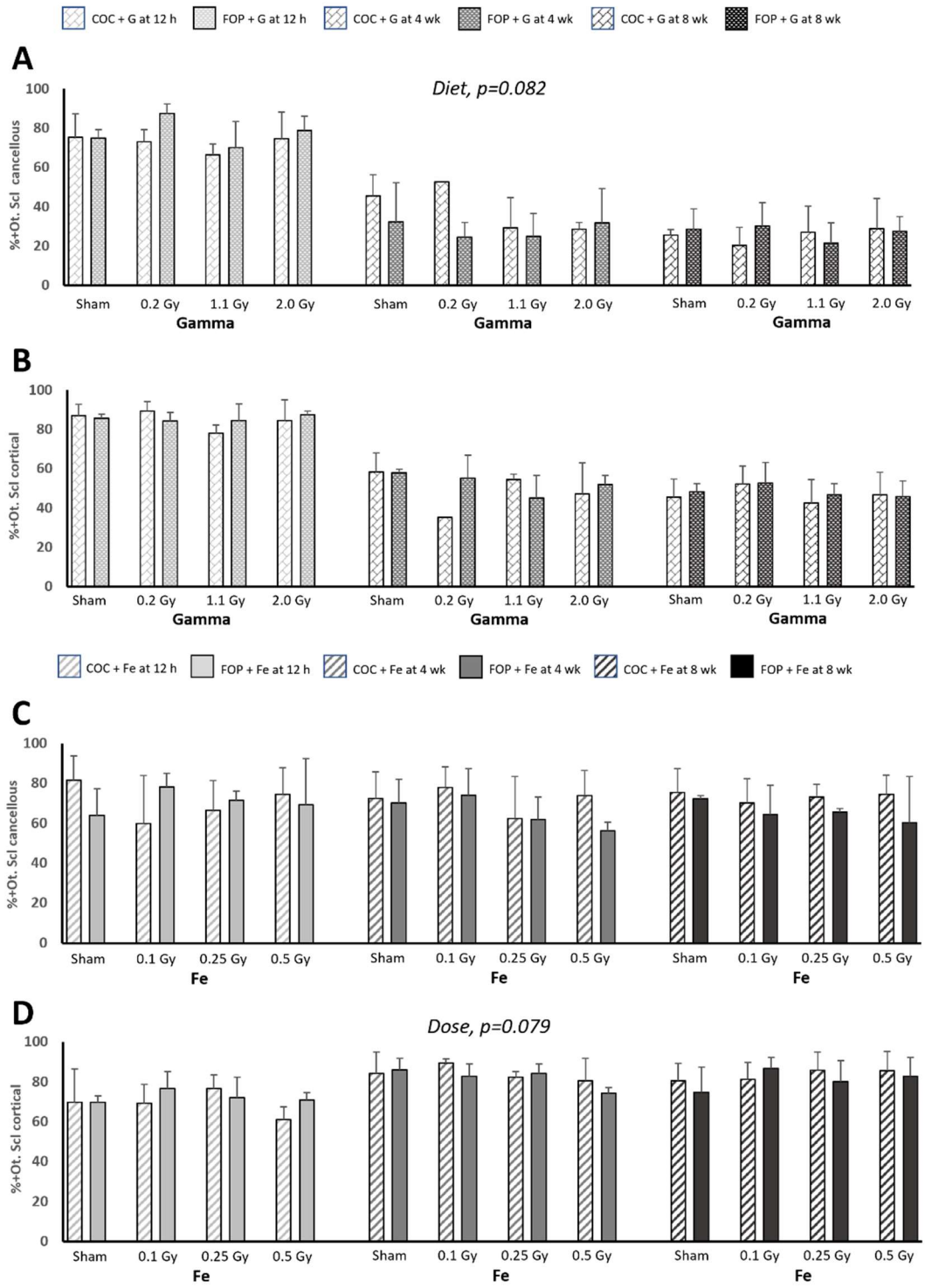

Figure 2-7. Percentage of osteocytes staining positive for sclerostin 12 hours, 4 weeks, and 8 weeks post exposure to γ radiation in cancellous (A) and cortical bone (B) and ^{56}Fe in cancellous (C) and cortical bone (D).

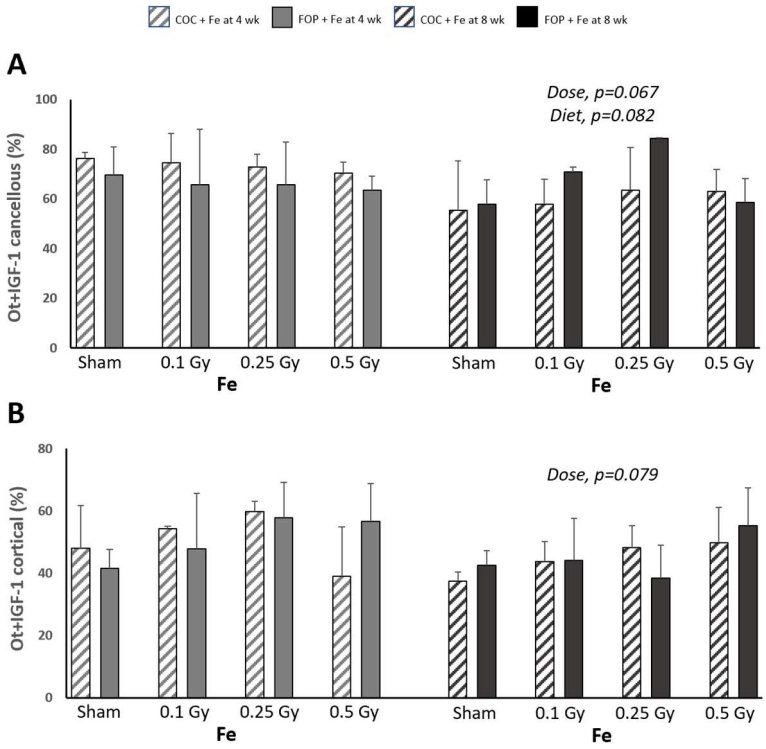

Figure 2-8. Percentage of osteocytes staining positive for IGF-1 at 4- and 8-weeks post exposure to ^{56}Fe radiation in cancellous (A) and cortical bone (B).

2.2.4. Marrow Adipocyte Quantification

Iron: No significant interactions or effects were detected in AV/TV or average adipocyte area at 4 or 8 weeks in mice exposed to ^{56}Fe (Figure 2-9 A-D). Adip.N at 4 weeks showed a significant effect of *dose* (p=0.096) such that adipocyte number was highest across diet at the highest dose of ^{56}Fe.

2.2.5. Histomorphometric Analysis of Relative Osteoid and Osteoclast Surfaces

Gamma: No significant interactions or effects were detected in OS/BS at 4 weeks or Oc.S/BS at 4- or 8-weeks post exposure to γ radiation (Figure 2.10 A-B). At 8 weeks, a significant interaction of *diet x dose* (p=0.072) was found in OS/BS, such that in FOP-

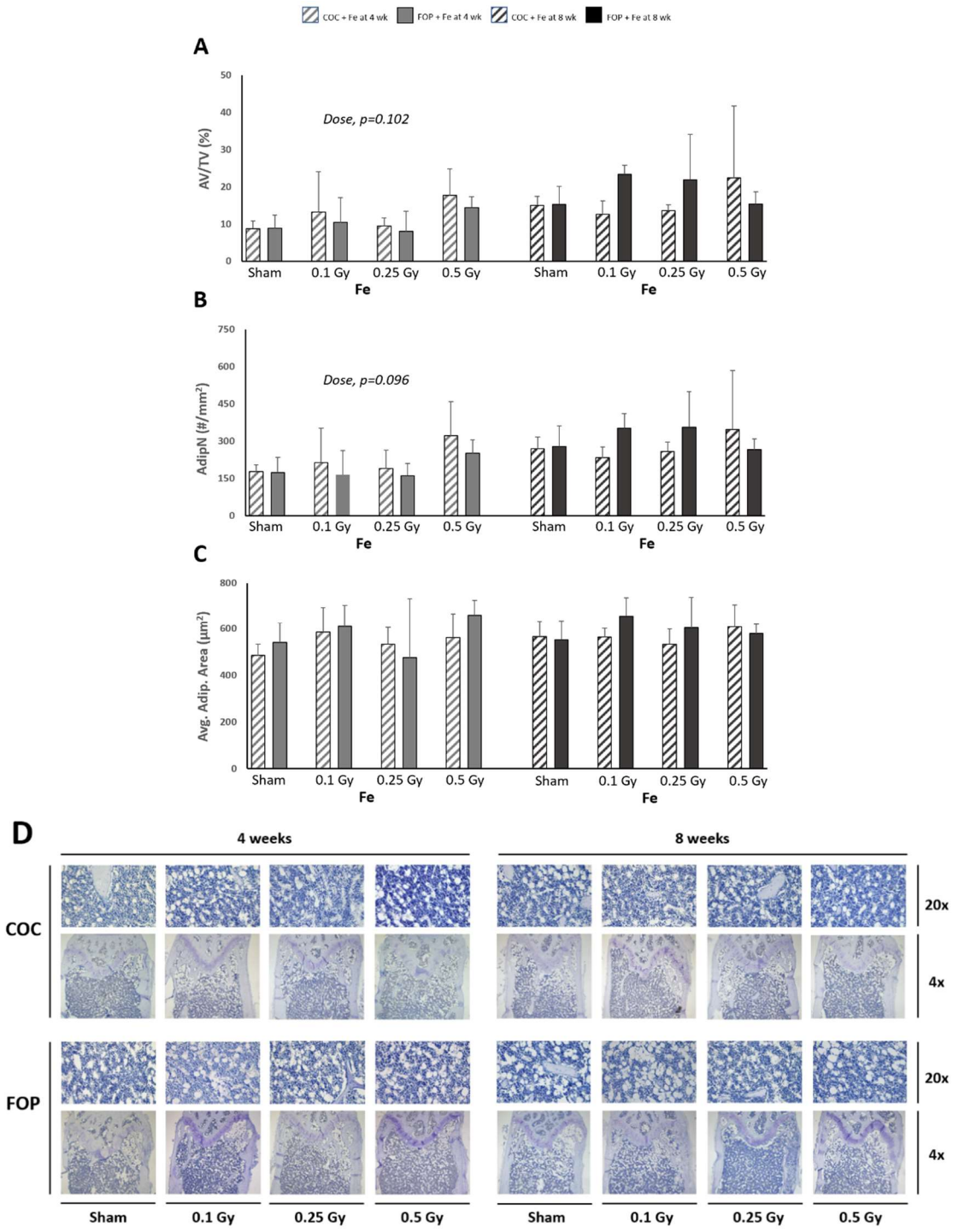

Figure 2-9. Quantification of marrow adiposity 4 weeks, and 8 weeks post exposure to ^{56}Fe radiation at the femoral metaphysis via adipocyte volume/total volume (A), adipocyte number per mm^2 (B) and adipocyte area (µm^2) (C). Representative images at 40 and 200x (D).

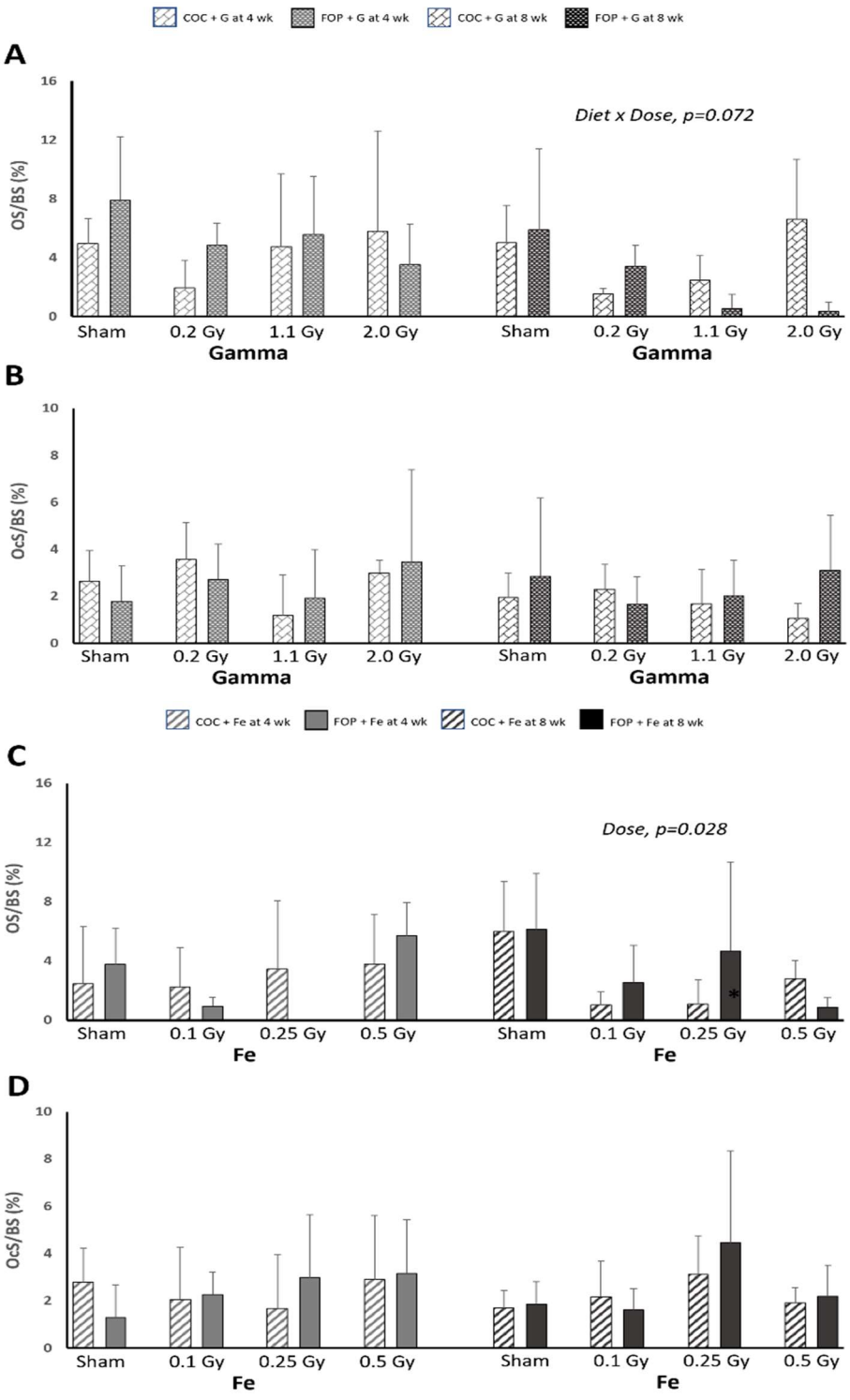

Figure 2-10. Assessment of osteoid and osteoclast surface relative to bone surface 4- and 8-weeks post exposure to γ (A, B) and ^{56}Fe radiation (C, D).

fed mice, OS/BS decreases as dose increases and in COC-fed mice, OS/BS increases with dose.

Iron: No significant interactions or effects were detected in OS/BS at 4 weeks or OcS/BS at 4- or 8-weeks post exposure to ^{56}Fe (Figure 2.10 C-D). At 8 weeks, a significant effect of *dose* ($p=0.028$) was found in OS/BS, such that OS/BS generally decreases as dose increases, except in FOP-fed mice with exposure to 0.25 Gy ^{56}Fe.

2.3. Discussion

We hypothesized that a diet high in omega-3 fatty acids would mitigate radiation-induced bone loss by reducing the generation of inflammatory cytokines in bone osteocytes and serum. Interestingly, we observed very little to no negative impact of these radiation exposures on bone mass and microarchitecture up to 8 weeks after exposure. In fact, at the lower doses (0.1 and 0.25 Gy) of ^{56}Fe, FOP-fed mice exhibited gains in diaphyseal cortical bone area and thickness at 4 weeks. These gains were not maintained at 8 weeks following exposure, though periosteal and endocortical diameters remained larger for those two doses in FOP-fed mice. These findings suggest that new bone formed at the periosteal surface was maintained even as some bone was lost at the endocortical envelope, as evidenced by larger endocortical diameters. Further, exposure to γ radiation in FOP-fed mice resulted in consistent gains in cortical thickness and area, with diet specific growth on medullary area and endocortical diameter.

Much of the previously published literature examining the impact of γ radiation on bone microarchitecture and geometry report significant detriments to cancellous bone

with minimal impact on cortical bone. Studies utilizing 1-2 Gy γ radiation have reported ~20% decreases in bone volume fraction, ~10% increase in trabecular separation, and mixed reports on decreased trabecular number and connective density (5, 41, 66) – these changes would likely be disadvantageous against compressive forces at the femoral metaphysis. Notably, these same studies report no impact of 0.1 or 0.5 Gy γ radiation on bone, in contrast to the data reported here elucidating a positive impact of 0.2-2.0 Gy γ radiation on both cancellous and cortical bone, particularly in mice fed a diet high in omega-3 fatty acids. Bokhari *et al*. reported similar positive impacts of γ radiation on bone in ~48-week-old female C57Bl/6 mice; it's important to note, in contrast to our study, this study utilized continuous, low dose, and low-dose rate methodologies totaling 0.175 Gy over 28 days, which may exert very different biological effects than acute exposures (9). Ours and Bokhari *et al.*'s findings are consistent with recently published data that space-relevant radiation may have neutral or even positive impacts on bone integrity (9, 10). A potential explanation for the differences in radiation impact on bone in our and Bokhari and colleagues work may be animal age at irradiation, as the majority of studies utilize animals less than 4 months in age (9, 10).

Studies investigating the impact of ^{56}Fe on bone outcomes primarily use doses over 1 Gy, which is more applicable to radiation exposure due to a solar flare than to that from GCR. Dosing of 2 Gy ^{56}Fe typically decreases cancellous bone volume fraction by ~31-34% with variable results on decrements to trabecular number and thickness, and connective density (2, 41). One study by Alwood *et al*. examined the impact of 0.5 Gy ^{56}Fe on 16-week-old male mice 5 weeks after irradiation (2); bone volume fraction

declined by ~16% relative to sham controls, with no other impact to cortical or cancellous parameters. Conversely, Bokhari *et al.* exposed 4 month old female mice to 0.5 Gy ^{56}Fe and found improved cancellous microarchitecture, specifically increases in bone volume fraction and trabecular number and thickness, 21 days post-exposure; cortical geometry was not assessed (10). Our study showed no impact to bone volume fraction at 4 or 8 weeks after exposure to up to 0.5 Gy ^{56}Fe across diets. Trabecular number and thickness were lower 8 weeks after radiation exposure in COC-fed mice and higher with increasing dose in FOP-fed mice. Connective density was also improved in FOP-fed mice at 8 weeks irrespective of dose. Surprisingly, cortical area and thickness, and endocortical diameter were higher as dose increased at 4 weeks post-irradiation. FOP-fed mice exhibited larger endocortical and periosteal diameters as radiation dose increased 8 weeks after exposure, which likely increases the resistance to bending at the diaphysis as a means to maintain mechanical strength. Together with data from Bokhari *et al.,* there appears to be a positive impact of low dose ^{56}Fe exposure to cancellous microarchitecture and cortical geometry. We also detected a modest long-term benefit of FOP on bone parameters after exposure to ^{56}Fe.

We did demonstrate, consistent with our hypothesis, that mice fed the FOP diet exhibited lower serum TNFα levels after ^{56}Fe exposure than that observed in COC-fed mice across radiation doses at all time points. Interestingly, γ irradiated mice on the FOP diet generally had higher serum TNFα than COC-fed mice. No published data exist on the impact of space-relevant doses of single ion irradiation, using γ or ^{56}Fe, on serum TNFα levels, nor on the combined impact of FOP and radiation.

Despite the key regulatory role of osteocytes in bone, no studies to date have described the osteocyte signaling response to space-relevant radiation exposure. Comparably, some studies have evaluated marrow cell gene expression in this context, which reflects an average response of multiple cell types, indicating increased marrow cell gene expression of TNFα in response to 2 Gy of γ radiation within 1 day of exposure, persisting up to three days post-exposure (1), with no change after exposure to 2.0 Gy of ^{56}Fe. In the current study, assessing the proportion of osteocytes positive for TNFα within bone, γ irradiated mice similarly showed a *diet x dose* effect on %+Ot-TNFα at 12 hours in cortical bone such that radiation exposure generally increased %+Ot-TNFα; though, unlike marrow cell gene expression of TNFα, this impact was still evident at 4 weeks in both cortical and cancellous bone. The FOP diet appeared to mitigate the radiation-induced increase, though only in cortical bone. Interestingly, ^{56}Fe exposed mice exhibited at a *diet x dose* effect on %+Ot-TNFα in both cancellous and cortical bone 12 hours after irradiation, with no differences at 4 or 8 weeks. Differences in our results versus previous studies may be due to the dose (2 Gy vs. 0.1-0.5 Gy ^{56}Fe), age (16 wks. Vs. 30-50 wks.), and/or sex (male vs. female), as well as the method of analysis (immunostaining vs. QT-PCR), among other factors.

Sclerostin, a downstream target of TNFα and a negative regulator of bone formation, would be expected to show a similar pattern to TNFα. However, sclerostin and *SOST* gene transcription are influenced by a number of proteins, such as RUNX2 and bone morphogenic proteins, which in turn can be influenced by radiation exposure. Gamma irradiated mice showed no differences in %+Ot-Scl between groups, though a

significant effect of *diet* was detected such that FOP-fed mice had a lower percentage of Scl-positive osteocytes. Macias *et al*. irradiated female mice with 0.17-1 Gy X-rays and did not detect changes in %+Ot-Scl at 3 weeks post-exposure (70). Surprisingly, in our study, ^{56}Fe mice at 4 weeks post showed a significant effect of *dose*, such that %+Ot-Scl decreased as dose increased, in cortical bone – a reduction in sclerostin signaling is typically associated with greater bone formation rates, which were not assessed in the current study. Macias *et al*. demonstrated that heavy ion exposure, using ^{28}Silicon, increased sclerostin-positive osteocytes in cortical bone (70). However, limited comparisons can be made as different strains of mice and different ion species were used.

Only FOP-fed mice exposed to ^{56}Fe exhibited increased %+Ot-IGF-1 in cancellous bone; however, in cortical bone, radiation exposure increased %+Ot-IGF-1 irrespective of diet. IGF-1 is increased in serum 8 weeks post-exposure to 1.6 Gy ^{56}Fe (107) and may be indicative of an anabolic effect in bone (75). This outcome is consistent with the modest improvement in microarchitecture observed in ^{56}Fe-exposed FOP-fed mice and may play a role mechanistically. Recent evidence has suggested that low dose radiation may be beneficial for bone, specifically as assessed 3 weeks after exposure to 0.5 Gy ^{56}Fe (10), though longer-term effects have not been elucidated. Further, few studies have evaluated the impact of space-relevant radiation on IGF-1 and bone. More research is required to determine the role of IGF-1 and osteocyte signaling in the bone response to radiation.

Few data exist on the response of bone marrow adipose tissue to space relevant radiation. In this study, number of adipocytes per mm^2 increased as ^{56}Fe dose increased, irrespective of diet. Clinical doses of radiation used in cancer therapy (e.g. 8 Gy) lead to increases in marrow adipocyte number, but not size, suggesting a possible increase in adipogenic capacity without an increase in fat storage (21). Radiation exposure may damage stem cell progenitors in the bone marrow niche, potentially causing a damage-induced increase in adipogenic capacity as a result of pushing stem cell differentiation away from osteogenesis and towards adipogenesis (18). Acute exposure to 1 Gy of γ radiation decreased adipocyte differentiation, assessed via decreased number of colony forming units, at three days post-exposure, but increased differentiation at three weeks post (66), suggesting only a transient decrement in adipogenic capacity. However, it remains unknown if chronic exposure to low dose radiation impacts adipogenic capacity in the same manner.

Osteoclast activity is significantly increased at 3 days post-exposure to 2 Gy of x-rays, but decreased by 1 week post (121–123). Similarly, Lima *et al*. demonstrated increased primary osteoclast differentiation, assessed via increased number of colony forming units, alkaline phosphatase activity, and number of mineralized nodules, at 3 days after exposure to 1.0 Gy of x-rays, which was no longer apparent at 3 weeks (66). Our data reveal no differences in relative osteoclast surface at 4- or 8-weeks after exposure to γ and ^{56}Fe, supporting previous data suggesting that the increase in osteoclast activity is likely transient following acute exposure.

At 8 weeks in all ^{56}Fe irradiated mice, relative osteoid surface was lower as radiation dose increased, which is consistent with data supporting decreases in osteoblast production and differentiation following irradiation, leading to decreased mineralization and osteoid surface (122, 123). Interestingly, at 8 weeks post-exposure in γ irradiated mice, COC-fed mice exhibited increased relative osteoid surface with radiation dose, while FOP-fed mice showed an inverse relationship. Mechanistically, it is unclear why FOP-fed mice have lower relative osteoid surface, indicative of depressed bone formation, after radiation exposure than COC-fed mice. These same mice exhibited significant improvements in cancellous microarchitecture, suggesting either increased bone formation and/or decreased bone resorption activity sometime after radiation exposure. Further, high dietary omega-3 fatty acid intake is usually associated with attenuated reductions in bone mineral density and reduced inflammation (7, 118).

There exist several limitations to this study. First, due to the extensive breeding challenges, there is a relatively small number of animals per group. A larger number per group would improve the applicability and statistical power of this study and should be considered for future experiments. Second, due to methodological limitations in space radiation research, ion species must be simulated separately. A mixed beam with more precise approximations of GCR composition would a more accurate simulation of actual GCR effects on bone outcomes; however, this is not currently feasible for the high-energy ion species in one exposure, nor for continuous exposures. Third, anticipated GCR exposure during future planetary missions will involve continuous exposure to HZE ions at very low dose rates. Currently, it is impossible to expose animals to HZE

ions generated only in accelerator beams for hours or days at a time. Differences in dose rates across minutes to days alters the biological impact of radiation exposure, as acute and chronic inflammatory responses may lead to different long-term outcomes. For example, our lab has previously shown an anabolic effect of very low dose-rate, continuous gamma, in contrast to literature demonstrating significant detriments after exposure to 2.0 Gy gamma radiation (9, 10, 41, 122). As technology progresses, the ability for research to more closely mimic space-relevant radiation will undoubtedly improve. Lastly, bone loss occurs with aging, leading to low baseline bone volumes in older animals, like those used in this study (35). Low bone volumes can mask differences between groups, as well as experimental impacts (12).

Despite these limitations, this study provides valuable new information. First, it provides important preliminary data on the role of osteocytes in the radiation-induced inflammatory response, which is largely unknown. This study is the first to describe osteocyte signaling in response to space-relevant doses of γ and ^{56}Fe radiation. Second, the capacity for a diet high in omega-3 fatty acids to mitigate the inflammatory response in the context of radiation exposure has not been characterized. This study is the first to elucidate, at a microscopic level, the impact on bone parameters. Further research should be done to elucidate the impact of FOP and radiation on bone outcomes in male mice, with continuous radiation exposure, and with mixed ion radiation, among others. In conclusion, we did not generally demonstrate a negative impact of acute, low-dose exposure to γ or ^{56}Fe radiation, though we did demonstrate mitigation of increased serum levels of TNFα with a diet high in omega-3 fatty acids.

3. DIET ALTERATIONS, WITH AND WITHOUT FECAL MICROBIAL TRANSPLANTS, TO RESCUE BONE QUALITY IN DIET-INDUCED OBESITY

The purpose of Study 2 (S2) was to determine if alterations in diet, with and without supplementation of microbiota from healthy mice, can rescue bone quality. These aims seek to explore the ability for diet and microbiota supplementation to reverse the negative effects of a pro-inflammatory obesogenic diet on bone. We hypothesized that a change in diet to a low-fat diet, in conjunction with microbiota supplementation, can mitigate the negative impacts of diet-induced obesity on bone in exercising mice. The sections below detail the methodologies that have been performed.

3.1. Methods

Male 5-week-old C57BL/6J mice (n=10/group) were purchased from Jackson Laboratories (Bar Harbor, ME) and randomly assigned to low-fat (LF) or high fat, high sugar (HFS) diets for 12 weeks (Figure 3-1). All mice were provided access to a running

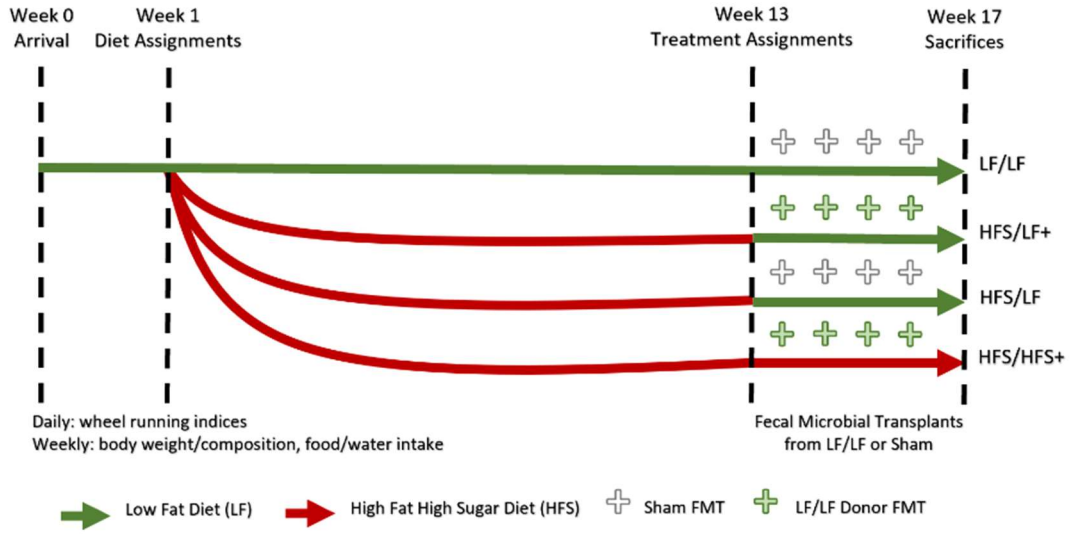

Figure 3-1. S2 Experimental Timeline

wheel. After 12 weeks on initial diet assignments, HFS-fed mice were subsequently randomized to one of three treatment groups for the next 4 weeks: LF diet with fecal microbial transplants (FMT) (HFS/LF+), LF diet with sham FMT (HFS/LF), and HFS diet with FMT (HFS/HFS+). Mice originally on the LF diet (LF/LF) were assigned to receive sham FMT's and remained on the LF diet. Treatment groups are designed to investigate the impact of combined diet alterations and supplementation with "healthy" microbes, diet alterations only, and supplementation with "healthy" microbes only, respectively. Body mass and composition, food and water intake, and fecal pellets were collected weekly and wheel running indices were assessed daily. Animals were terminated at 23 weeks of age.

This study was approved and followed procedures set by the Texas A&M Institutional Animal Care and Use Committee. All animals were individually housed in the university vivarium with 12-h light/dark cycles.

3.1.1. Diet

Animals were randomly assigned to one of two *ad libitum* diets: a standard rodent, low-fat (LF) diet consisting of 4% fat, 25.2% protein, 39.5% carbohydrate, 3.3% crude fiber, and 10% neutral fiber (Diet 8604, Harland Labs, Houston, TX) or a high fat, high sugar (HFS) diet consisting of 45% fat, 20% protein, 35% carbohydrate, and 5% fiber, with a 20% fructose solution as a replacement of regular drinking water (Diet D12451, Research Diets, Inc., New Brunswick, NJ). The HFS diet is intended to simulate a diet composition worse than the average United States citizen in terms of fat and sugar content. The average US citizen's diet is composed of ~48.5% carbohydrate,

~15.5% protein and ~33% fat, with ~10% of total calories coming from fructose (20, 77). High fat and fructose-rich diets have independently been shown to exert a negative impact on bone biology, but no studies to date have examined the combined effect using an overfeeding model. The control, low-fat diet utilized in this study is the standard chow diet provided by the University Vivarium and is designed to provide the necessary nutrients to maintain animal health.

Caloric intake was assessed at the beginning and end of each week by weighing food and fluid intake using an electronic scale. Calories from fluid intake were converted for regular drinking water as 0 kcal per gram and for the 20% fructose solution as 0.8 kcal per gram. Total caloric intake (kcal) was assessed for the 4-week treatment period (Week 13-Week 17) by summing calories from food and fluid intake.

3.1.2. Voluntary Wheel Running

All mice were provided access to a running wheel for the duration of the study. Voluntary wheel running is a commonly used methodology in rodents, akin to aerobic exercise in humans (29). Unlike forced treadmill running, voluntary wheel running leads to improved aerobic health without inducing a chronic stress response (24).

Running wheels had a 410 mm circumference and solid running surface (Kaytee, Chilton, WI, USA). Bicycle computers (BC8.12, Sigma Sport, Batavia, IL, USA) were attached to the top of the animal cage with the magnetic sensor pointing downwards towards the running wheel and a magnet was glued to the outside rim of the running wheel. Activity data, specifically distance (km/day), duration (min/day), and

speed(m/min) were recorded every 24 hours for the duration of study. Wheels were assessed for proper function and sensor alignment daily.

3.1.3. Body Composition

Body weight and composition were assessed weekly in all mice in S2 beginning at 5 weeks of age. Body weight was assessed using an electronic scale. Body composition, specifically fat and lean mass, were assessed weekly using an MRI designed for use in rodents (EchoMRI, Texas, USA).

3.1.4. Fecal Pellet Collection & Microbial Transplantation

During weekly body composition assessments, fresh fecal pellets were collected. Mice were placed individually into empty, sterilized cages and pellets were collected in sterile cryotubes immediately after passing. Cryotubes were then flash frozen and stored at -80°C. Fecal pellet collection was completed weekly for the duration of the study.

At the onset of the treatment period at Week 14, mice were randomly assigned to receive FMT's from donor mice or a sham transplant using buffer solution only for 4 weeks. Transplants were conducted at the start of each week for the duration of the treatment period, resulting in a total of 4 transplants per mouse. Fecal pellets used in the FMT were collected from the mice continuously assigned to the LF diet (LF/LF). One pellet from each donor mouse (n=10) was mixed in an anaerobic tube filled with 500 ml of pre-reduced phosphate buffered saline and cysteine. The fecal solution (150 µl) was inserted into the stomach of each mouse assigned to the transplant groups via oral gavage. Mice assigned to receive sham FMT's were given pre-reduced phosphate

buffered saline and cysteine (150 µl) via oral gavage to match the stress incurred from additional handling and stomach filling.

3.1.5. Euthanasia & Tissue Collection

Animals were euthanized using 3-4% isoflurane inhalation followed by cervical dislocation. Left and right femora and tibiae were collected and stored appropriately for analyses. Whole and proximal femora collected for mechanical testing and micro-computed tomography were wrapped in gauze soaked in phosphate-buffered saline and stored at -20°C. Whole tibiae and distal femora collected for histology were fixed in 4% phosphate-buffered formalin for 24 hours and subsequently stored in 70% ethanol at 4°C.

3.1.6. Micro-computed Tomography

Micro-computed tomography (µCT) was performed at the distal metaphysis and mid-diaphysis of the right femur using a high-resolution imaging system (Sky Scan 1172, Bruker, Massachusetts, USA) to assess bone geometry and microarchitecture. Distal and mid-diaphyseal femora regions were scanned at 6 µm isotropic voxel size using a 0.5 aluminum filter. Analysis of cancellous microarchitecture was performed with a 1 mm region beginning proximal to the growth plate and excluding cortical bone. Cancellous bone parameters analyzed include bone volume fraction (BV/TV; %), trabecular thickness (Tb.Th; mm), trabecular number (Tb.N; mm^{-1}), and trabecular spacing (Tb.Sp; mm). Analysis of cortical geometry was assessed across 5 slices located ~2.5 mm proximal to the growth plate in the distal femur. Cortical bone parameters analyzed include cortical area (Ct.Ar; mm^2), cortical thickness (Ct.Th; mm), and polar

moment of inertia (pMOI; mm^4). Scan acquisition and analyses were conducted according to established guidelines for use of μCT in rodents (12).

3.1.7. Mechanical Testing

Mechanical testing was performed using a standard desktop test machine sized for rodent bone (Instron 3345, Instron, Massachusetts, USA) to assess femur mechanical properties at the mid-diaphysis via 3-point bending to failure and at the femoral neck via compressive loading. Load–displacement data were recorded at 50 Hz and analyzed using Bluehill software (v2.14.582, Instron Bluehill, Massachusetts, USA). Data were processed *post hoc* using a custom-written MATLAB program (R2015a v8.5.0.197613, The MathWorks, Inc., Massachusetts, USA) to generate outcomes using force–displacement curves. Prior to mechanical testing, bones were thawed at room temperature.

3.1.7.1. 3-Point Bending to Failure

Anterior-posterior and medial-lateral diameters at the mid-diaphysis of femora were measured using digital calipers. Femora were placed on two lower metal support pins, ~10 mm apart, with the upper loading pin centered on the mid-diaphysis. Quasi-static loading was applied to the mid-diaphysis at a displacement rate of 2.5 mm/min, at 50% of total bone length, with a 100-N load cell until complete fracture. Load displacement data was collected to assess structural (stiffness, N/mm; maximum force, N; yield force, N; energy to yield, mJ; energy to fracture, mJ) and material (elastic modulus, GPa; yield stress, MPa; ultimate stress, MPa; toughness, mJ/mm^3) properties. MATLAB analysis determined the structural variables described above. Stiffness was

defined to be the slopes of the elastic linear portion of the loading curve. Maximum force was designated as the largest force achieved throughout the test. Parameters relating to energy-absorbed were determined as the area under the load–displacement curve. Material properties were estimated by normalizing structural properties for bone geometry using the mid-diaphysis bending cross-sectional moment of inertia (CSMI), the anterior-posterior surface diameter at the mid-diaphysis, and the support span distance. CSMI was estimated as half of pMOI determined by μCT. Classical beam theory was applied to estimate the material properties.

3.1.7.2. Femoral Neck Compression Test

Proximal femora were placed in machined holes matched to bone size in a rigid, aluminum fixture, such that the femur was secured up to the lesser trochanter and oriented with the main axis of the shaft, oriented vertically, throughout the test. Quasi-static loading was applied to the femoral head through a flat cylindrical platen in a direction parallel to the femoral shaft at a displacement rate of 2.5 mm/min until complete fracture. Load displacement data was collected to assess maximal compression strength (N).

3.1.8. Static Histomorphometry

Static histomorphometry was performed at the distal femoral metaphysis [dynamic indices of bone formation activity could not be collected to prevent excessive stress to the animals, given stress induced via oral-gavage, and wheel-running indices as the primary outcome of the parent study]. Distal femora were subjected to serial dehydration and embedded in methyl methacrylate (Sigma-Aldrich, Missouri, USA).

Longitudinal sections were cut to approximately 5 μm thickness using a Leica microtome (RM 2255, Leica, Wetzlar, Germany), mounted on gelatinized slides and baked for ~48 hours at 37°C. Slides were subsequently treated with von Kossa stain and tetrachrome counterstain to assess osteoid (OS/BS, %) and osteoclast surfaces (OcS/BS, %), relative to total cancellous bone surface. Histomorphometric analyses were performed using OsteoMeasure Analysis System, version 3.3 (OsteoMetrics, Inc., Georgia, USA) interfaced with a light microscope and CCD camera (DP73, Olympus, Tokyo, Japan). A defined region of interest was established starting ~500 μm from the growth plate and within area of ~4 mm^2 at a magnification of 400x (See Fig. 2-2).

3.1.9. Immunohistochemistry

Right tibiae were decalcified in a sodium citrate/formic acid solution for approximately 12 days prior to dehydration and processing using a Thermo-Scientific STP 120 Spin Tissue Processor and were paraffinized via a Thermo Shandon Histocenter 3 Embedding tool. Longitudinal sections were cut to approximately 5 μm thickness using a Leica microtome (RM 2255, Leica, Wetzlar, Germany), mounted on positively charged slides and baked overnight at 37°C. Slides were later stained for proteins of interest using an avidin-biotin method. Briefly, heat-mediated antigen retrieval was performed when specified by manufacturer instructions using 1% triton in phosphate-buffered saline. Samples were rehydrated, peroxidase inactivated using 3% H_2O_2/methanol, permeabilized using 0.5% Triton-X 100 in phosphate-buffered saline, blocked with species-appropriate serum for 30 minutes at room temperature (Vectastain Elite ABC; Vector Laboratories, California, USA) and incubated overnight at 4°C with

primary antibodies: polyclonal rabbit anti-TNFα (1:200; Abcam, Cambridge, UK), polyclonal goat anti-Sclerostin (1:150; R&D Systems, Minnesota, USA), polyclonal rabbit anti-IGF-1 (1:200; R&D Systems, Minnesota, USA), and polyclonal goat anti-IFNγ (1:150; R&D Systems, Minnesota, USA). Sections were incubated at room temperature for 45 minutes with species-appropriate biotinylated anti-IgG secondary antibody. Peroxidase development was performed with an enzyme substrate kit (diaminobenzidine [DAB]; Vector Laboratories, California, USA). Counterstaining was conducted with methyl green counterstain (Vector Laboratories, California, USA) for 2.5 minutes. Sections were then dehydrated into organic phase and mounted with xylene-based mounting media (Polysciences, Pennsylvania, USA). Negative controls for all antibodies were completed by omitting the primary antibody. Immunohistochemical analyses were performed using OsteoMeasure Analysis System, version 3.3 (OsteoMetrics, Inc., Georgia, USA) interfaced with a light microscope and CCD camera (DP73, Olympus, Tokyo, Japan). The proportion of all osteocytes stained positively for proteins of interest were quantified in the cancellous bone, starting ~500 μm from the growth plate and within area of ~4 mm^2, and in the cortical bone at mid-diaphysis, within an area of ~1 mm^2 per side, at a magnification of 400x (See Fig. 2-3).

3.1.10. Marrow Adipocyte Quantification

Right tibiae were collected, decalcified, paraffinized and sectioned as described in the preceding section. Slides were subsequently treated with hematoxylin (Vector Laboratories, California, USA) counterstain to measure adipocyte number (#/mm) and average adipocyte size (μm^2). Briefly, slides were rehydrated, counterstained with

hematoxylin for 30 seconds, rehydrated and mounted using xylene-based mounting media (Polysciences, Pennsylvania, USA). Histomorphometric analyses were performed using OsteoMeasure Analysis System, version 3.3 (OsteoMetrics, Inc., Georgia, USA) interfaced with a light microscope and CCD camera (DP73, Olympus, Tokyo, Japan). A defined region of interest was established starting ~500 μm from the growth plate and within area of ~4 mm^2 at a magnification of 200x (See Fig. 2-4).

3.1.11. Statistical Approach

Statistical analyses were performed on all outcome measures using a two-way ANOVA (factors = diet, treatment). An alpha level of 0.05 was set *a priori* to achieve sufficient power (β=0.80) with an *n* of 10 per group. Tukey's *post-hoc* test was employed if the p-value was less than or equal to 0.05.

3.2. Results

Data on body mass, body composition, caloric intake, wheel running indices, and microbiota are reported in full in the dissertation of Ayland C. Letsinger (63). Briefly, total body weight (TBW) and fat mass (FM) at termination were ~26% and ~270% higher, respectively, in HFS/HFS+ mice, as compared to mice switched from the HFS diet, and ~41% and ~440% higher, respectively, versus LF/LF mice ($p<0.001$). HFS/LF+ and HFS/LF mice reduced TBW by ~20% and FM by ~60 versus LF/LF and HFS/HFS+ mice ($p<0.001$) from Week 13 to Week 17. Total caloric intake from Week 13-17 was reduced in HFS/LF+ and HFS/LF mice by ~20% versus LF/LF and ~40% versus HFS/HFS+, with HFS/HFS+ consuming ~30-60% greater calories per day than all other groups ($p<0.018$). Wheel running indices reveal increases (% change from

Week 13-17) in duration (+55-85%), distance (+40-94%), and speed (+20-29%) in HFS/LF+ and HFS/LF mice compared with LF/LF and HFS/HFS+ mice ($p<0.011$). At Week 13, microbial composition in LF/LF mice differed from all other groups. At Week 17, microbial composition in groups switched to the LF diet were consistent with that of continuously LF-fed mice at termination, while microbial composition differed in continuously HFS-fed mice. In sum, mice switched from the HFS diet exhibited significant reductions in TBW, FM, and total caloric intake and increases in running distance, duration, and speed, while continuous LF and HFS-fed mice maintained these metrics.

3.2.1. Micro-computed Tomography Assessment of Bone Geometry and Microarchitecture

Cancellous microarchitecture and cortical geometry were improved only in mice continuously fed the HFS diet, with gain of cancellous bone mass of greater magnitude. Trabecular BV/TV (+85-108%, $p<0.001$), Tb.Th (+14-19%, $p<0.001$), and Tb.N (+50-75%, $p<0.001$) were higher and Tb.Sp (-17-19%, $p<0.001$) was lower in HFS/HFS+ compared to all other groups (Figure 3-2 A-D At the mid-diaphysis, LF/LF mice had ~8% lower T.Ar versus HFS/HFS+ mice only ($p=0.022$) and ~17% lower pMOI versus all groups ($p=0.008$) (Figure 3-3 A,C). Ct.Th was not different among groups ($p=0.068$) (Figure 3-3 B). Interestingly, groups switched from the HFS diet were consistent with continuously LF-fed mice on all cancellous and cortical parameters, except pMOI, where these mice maintained higher pMOI consistent with continuously HFS-fed mice.

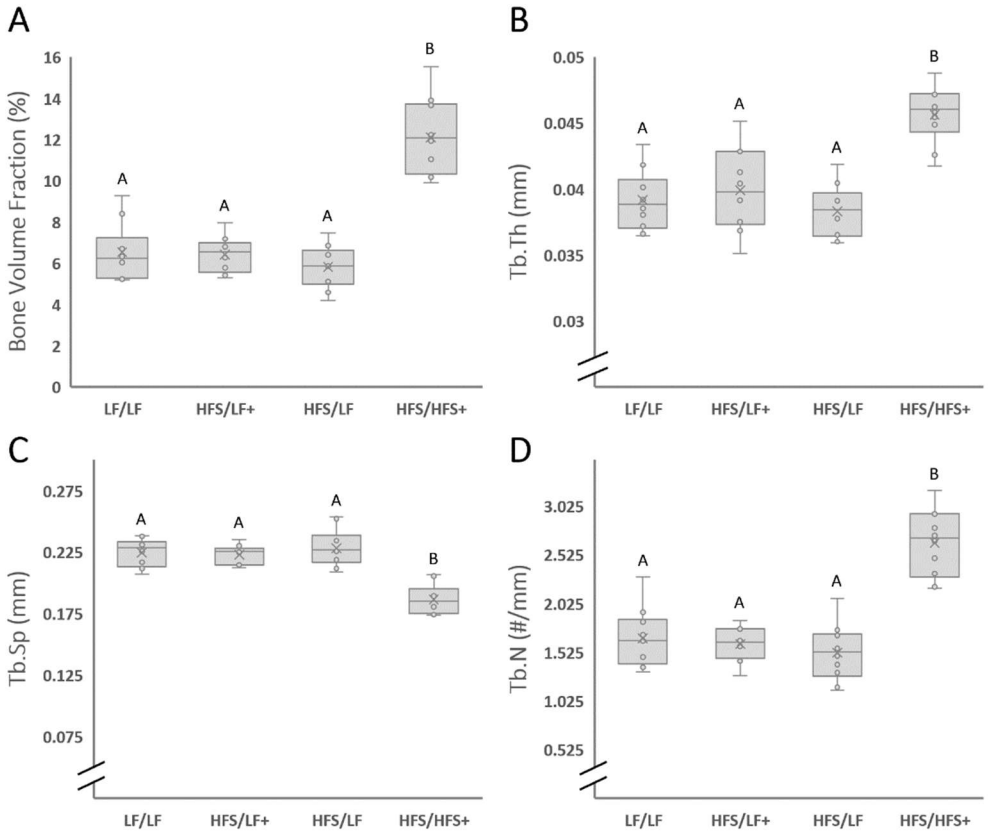

Figure 3-2. Cancellous microarchitecture at the distal femoral metaphysis. A) Bone volume/total volume, BV/TV (%); B) Trabecular Thickness, Tb.Th (mm); C) Trabecular Separation, Tb.Sp (mm); D) Trabecular Number, Tb.N (#/mm).

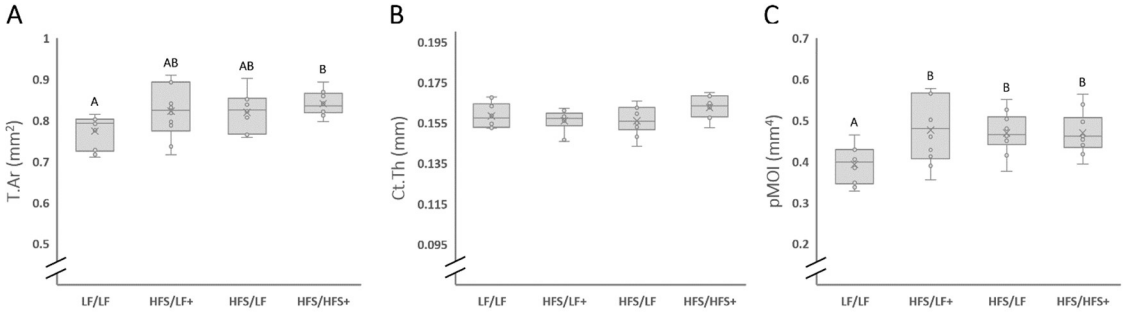

Figure 3-3. Cortical geometry at the femoral diaphysis. A) Total area, T.Ar (mm^2); B) Cortical Thickness, Ct.Th (mm); C) Polar Moment of Inertia, pMOI (mm^4).

3.2.2. Material and Structural Properties at the Mid-Diaphysis and Femoral Neck

HFS/HFS+ mice had ~20% higher maximal compressive load at the femoral neck compared to HFS/LF and HFS/LF+ mice ($p<0.003$), with no difference compared to LF/LF mice (Figure 3-4).

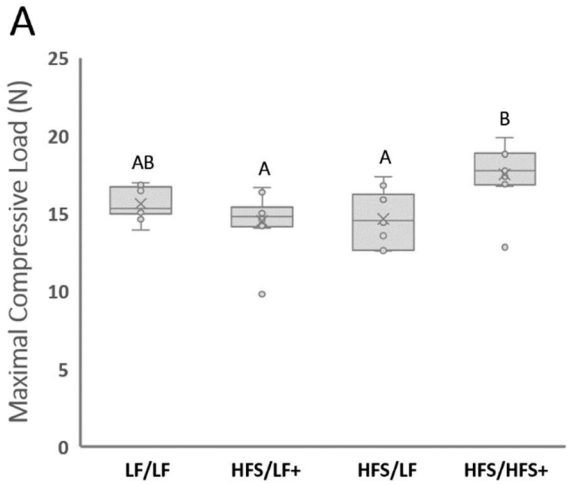

Figure 3-2. Femoral Neck Compression, assessed as maximal compressive load (N).

Maximum strength (N) at the femoral diaphysis was 15-17% higher in HFS/HFS+ mice compared to all other groups ($p<0.021$) (Table 3-1). Stiffness (N/mm) was high~20% higher in HFS/HFS+ mice relative to HFS/LF mice only ($p=0.007$), with no difference between LF/LF ($p=0.120$) or HFS/LF+ mice ($p=0.063$). No differences were detected between groups in yield force (N), energy to yield (mJ) or energy to fracture (mJ). Elastic modulus (GPa) was ~18-22% lower in HFS/LF and HFS/LF+ versus LF/LF ($p<0.038$), though not different from HFS/HFS+ mice. Ultimate stress (MPa) was ~~~16% lower in HFS/LF mice versus LF/LF ($p=0.034$), though not different from HFS/LF+ (~14%, $p=0.066$) or HFS/HFS+ mice. Yield stress (MPa) was

22% lower in HFS/LF+ mice compared to LF/LF mice only (p=0.038). No differences were detected among groups in toughness (mJ/mm^3).

Table 3-1. Mid-diaphyseal femur 3-point bending to failure, assessing structural and material mechanical properties.

	LF/LF	HFS/LF+	HFS/LF	HFS/HFS+	
Structural Properties					
Maximum Force (N)	19.63 ± 2.02^{A}	19.82 ± 2.07^{A}	19.25 ± 1.9^{A}	22.68 ± 2.37^{B}	**p=0.003**
Stiffness (N/mm)	92.98 ± 9.24^{AB}	91.44 ± 14.05^{AB}	86.86 ± 12.29^{A}	104.7 ± 9.49^{B}	**p=0.010**
Yield Force (N)	9.49 ± 1.95	8.76 ± 0.92	9.08 ± 1.11	10.15 ± 1.23	p=0.143
Energy to Yield (mJ)	0.537 ± 0.250	0.458 ± 0.105	0.511 ± 0.129	0.525 ± 0.106	p=0.692
Energy to Fracture (mJ)	8.47 ± 3.28	6.96 ± 1.83	8.61 ± 2.42	7.54 ± 2.11	p=0.401
Material Properties					
Elastic Modulus (GPa)	3.420 ± 0.472^{A}	2.797 ± 0.515^{B}	2.666 ± 0.407^{B}	3.243 ± 0.573^{AB}	**p=0.004**
Ultimate Stress (MPa)	114.9 ± 11.87^{A}	98.57 ± 14.74^{AB}	96.74 ± 10.89^{B}	112.2 ± 18.36^{AB}	**p=0.011**
Yield Stress (MPa)	56.04 ± 13.65^{A}	43.86 ± 8.16^{B}	45.79 ± 7.36^{AB}	50.05 ± 8.32^{AB}	**p=0.039**
Toughness (mJ/mm^3)	0.50 ± 0.23	0.37 ± 0.10	0.42 ± 0.12	0.41 ± 0.09	p=0.263

3.2.3. Histomorphometric Analysis of Relative Osteoid and Osteoclast Surfaces

No differences in OS/BS, a marker of bone formation, (p=0.408) or OcS/BS, marker of bone resorption, (p=0.059) were found among groups (Table 3-2).

Table 3-2. Static Histomorphometry. Osteoid surface and osteoclast surface relative to bone surface.

	LF/LF	HFS/LF+	HFS/LF	HFS/HFS+	
Osteoid Surface/Bone Surface (%)	5.44 ± 4.44	6.38 ± 2.74	3.99 ± 2.10	4.65 ± 3.36	p=0.408
Osteoclast Surface/Bone Surface (%)	0.75 ± 0.69	1.26 ± 0.70	1.22 ± 0.59	0.65 ± 0.40	p=0.059

3.2.4. Immunohistochemical Staining of Osteocytes Positive for Proteins of Interest

Immunostaining for TNFα, sclerostin, and IGF-1 in cortical and cancellous bone revealed no significant differences among groups (Table 3-3). The percentage of osteocytes positive for IFNγ in cancellous bone was ~24% and ~29% higher in HFS/LF+ and HFS/LF mice, respectively, compared to HFS/HFS+ mice ($p<0.019$), with no differences observed in cortical bone

Table 3-3. Immunohistochemistry. Percentage of osteocytes staining positive for TNFα, Sclerostin, IGF-1 and IFNγ in metaphyseal cancellous and diaphyseal cortical bone.

	LF/LF	HFS/LF+	HFS/LF	HFS/HFS+	
%Ot+TNFα					
Metaphyseal Cancellous	55.76 ± 12.08	64.58 ± 10.51	52.83 ± 17.41	54.91 ± 13.59	p=0.122
Diaphyseal Cortical	38.43 ± 7.55	40.81 ± 9.72	43.72 ± 8.49	37.17 ± 12.24	p=0.454
%Ot+Scl					
Metaphyseal Cancellous	77.64 ± 13.21	77.47 ± 12.67	78.77 ± 12.06	72.91 ± 7.27	p=0.681
Diaphyseal Cortical	83.04 ± 6.12	81.53 ± 9.94	80.38 ± 7.79	77.21 ± 4.68	p=0.355
%Ot+IGF-1					
Metaphyseal Cancellous	74.72 ± 7.39	71.98 ± 9.15	77.73 ± 9.25	77.85 ± 9.99	p=0.496
Diaphyseal Cortical	71.57 ± 12.52	66.84 ± 8.41	70.99 ± 6.85	73.64 ± 5.17	p=0.371
%Ot+IFN-γ					
Metaphyseal Cancellous	70.06 ± 9.58^{A}	79.13 ± 6.84^{A}	76.86 ± 8.23^{A}	61.49 ± 15.67^{B}	*p=0.005*
Diaphyseal Cortical	56.85 ± 6.55	61.71 ± 8.88	61.59 ± 12.05	53.55 ± 16.09	p=0.325

3.2.5. Marrow Adipocyte Quantification

HFS/HFS+ mice had ~40% greater marrow adipocyte size (μm^2) versus LF/LF mice ($p=0.002$), with no difference versus HFS/LF+ or HFS/LF mice (Figure 3-5). No difference was found in marrow adipocyte number (#/mm) among groups.

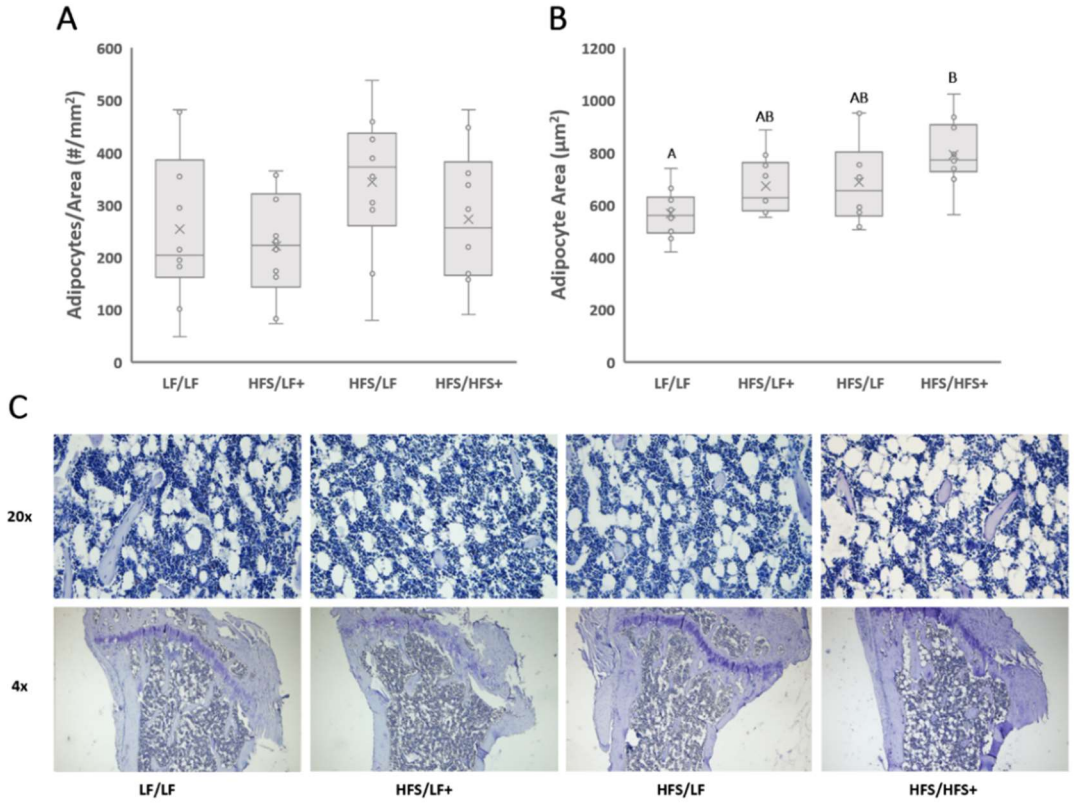

Figure 3-3. Bone Marrow Adiposity. A) Average number of adipocytes (1/mm^2); B) Average adipocyte area (µm^2); C) Representative images at 200x and 40x.

3.3. Discussion

Given the prevalence of diet-induced obesity via consumption of a high fat, high sugar diet, across the developed world, along with associated decreases in bone quality, it is important to understand the impacts of HFS feeding and potential therapeutic interventions. To this end, we hypothesized a change in diet from HFS to LF, in combination with the addition of "healthy" microbes, would rescue bone quality and strength from the detrimental impacts of an HFS diet in exercising mice. Interestingly, we found that HFS feeding resulted in remarkably large improvements in cancellous bone microarchitecture and structural mechanical properties. It is worth noting here that

continuously HFS-fed mice weighed nearly twice as much and exercise approximately half as much, in terms of distance, duration, and speed, compared to all other groups. Given body weight, it would be reasonable to assume that weight-induced mechanical loading is greater in continuous HFS-fed mice; however, exercise-induced mechanical loading is lower. It is unclear what the actual applied load to the bone is within these mice, and whether greater mechanical load or excess calories, or the combination, may be responsible. Despite improved bone quantity, but bone quality may be diminished as evidenced by the failure to improve femoral neck strength and material mechanical properties at the femoral diaphysis. Notably, diet alterations, with and without FMT's, appears to partially return the bone phenotype to match mice continuously fed the LF diet.

Cancellous microarchitecture, particularly bone volume fraction and trabecular number, improved to an unusually large degree in mice continuously fed the HFS diet. While cancellous microarchitecture improved only in continuously HFS-fed mice, all mice that received the HFS diet during the study retained a higher polar moment of inertia than that observed in mice continuously fed a LF diet. This is particularly interesting because polar moment of inertia increased despite no difference in cross-sectional area or cortical thickness at the diaphysis in mice switched off the HFS diet, compared to continuously LF-fed mice. Slightly higher cross-sectional area, despite non-significance, would require a larger radius of the cross-section, and thus likely explains the greater changes in polar moment of inertia, given it is calculated as the radius to the fourth power. Much of the literature in this area utilizes sedentary mice to compare the

impact of HF vs. LF feeding. In those studies, cancellous microarchitecture is typically negatively altered, specifically decreased bone volume fraction, trabecular number, and bone mineral density and increased trabecular separation, while cortical microarchitecture is improved, specifically increased cortical cross-sectional area and thickness (28, 46, 95, 111, 128). In exercising mice, however, no difference in cancellous microarchitecture have been consistently reported between LF and HF-fed mice (73, 105, 106). A primary difference between the methodologies used in those previous studies and those used here is the use of a high fat, high sugar diet and simulated sugar-sweetened beverages versus only high fat feeding. Unlike HF feeding, the HFS diet induces overfeeding, as assessed by significantly increased caloric intake in HFS versus LF mice, largely versus the addition of simulated sugar sweetened beverages (63). Further, both high fat and fructose-rich diets have been shown to independently impact skeletal biology at the molecular level, suggesting the combination may have an additive effect. Only one published study has investigated recovery of bone quality after HF feeding using diet alterations (95), but in sedentary mice. That research group found partial recovery in cancellous microarchitecture with diet alterations, but no recovery of cortical parameters (95). In contrast, in our study, exercising mice switched to a LF diet after 12 weeks of HF feeding exhibited a nearly complete reversal of the unusually large gains in cancellous bone volume and microarchitectural variables seen in continuously HFS-fed mice, while cortical parameters were largely maintained compared to mice continuously fed an HFS diet. These data suggest that, in exercising mice, HFS feeding promotes improvements in cancellous and cortical bone quantity. One potential

explanation for this is that the combination of mechanical loading via wheel running in the context of excess weight and/or increased caloric intake may further promote bone anabolism. In contrast, alterations in diet from HFS to LF led to significant reductions in total caloric intake, due to the loss of excess calories provided by the 20% fructose solution, and large increases in physical activity, likely resulting in a negative energy balance in these mice. A short-term energy deficit may have exacerbated the reversal of improved cancellous microarchitecture seen in continuously HFS-fed mice. A gradual diet transition may be able to mitigate any energy deficit and should be investigated.

Maximal compressive load (N) at the femoral neck significantly decreased in mice switched off the HFS diet, with and without FMT's, compared to continuously HFS-fed mice only. Interestingly, despite HFS/HFS+ mice weighing ~2x more than LF/LF mice, continuously fed HFS mice did not have greater maximal compressive load than mice continuously fed the LF diet, suggesting a failure to improve bone quality with HFS feeding. No studies to date have explored the impact of an HFS diet on femoral neck strength in exercising mice. However, a compositionally high fat, high sugar diet, utilizing sucrose as the sugar source, for 10 weeks significantly reduced maximal compressive load at the femoral neck in young sedentary male mice (45). Zernicke et al. utilized this same diet for 24 months in female rats and found relative femoral neck strength (N/g TBW) was significantly lower than that observed in animals on a standard chow diet (130), further supporting the concept that despite increased mechanical loading, bone quality may be diminished at the femoral neck in diet-induced obesity.

Structural properties at the femoral diaphysis were enhanced in mice continuously fed the HFS diet, while material properties were diminished in mice switched from the HFS diet. Maximum force at the femur significantly improved in mice continuously fed the HFS diet compared to all other groups, though stiffness improved only compared to mice switched from the HFS diet without FMTs (HFS/LF). Previous studies utilizing HF diets in exercising mice report no differences in mechanical properties between LF and HF-fed mice (73, 105), except for decreased stiffness in HF mice relative to LF (73). In the current study, elastic modulus was significantly higher in mice continuously fed the LF diet compared to mice switched from the HFS diet, with and without FMTs, though continuous HFS feeding did not lead to differences. In contrast, McCabe et al. showed decreased elastic modulus in exercising HF-fed mice versus LF-fed mice after 14 weeks. Ultimate and yield stress were also highest in our mice continuously fed the LF diet compared to HFS/LF and HFS/LF+, respectively. The apparent differential impact of diet alterations, with and without FMTs, on mechanical strength, whereby ultimate stress and maximum force are decreased only in HFS/LF mice while yield stress is decreased only in HFS/LF+ mice, is interesting and should be investigated further. In sedentary mice, diet alterations from HF to LF have been shown to partially rescue mechanical properties, specifically yield load, which is analogous to yield force reported here (95). However, our data show a positive impact of HFS-feeding and exercise on bone strength, while diet alterations appear to result in lower mechanical strength. It's important to note again here that mice switched from the HFS diet significantly reduced total body and fat mass, consumed significantly fewer calories, and

significantly increased physical activity in this 4-week span, while continuously LF- and HFS-fed mice remained relatively constant in these parameters. Ionova-Martin *et al*. reports diminished material properties with 19 weeks of HF feeding in sedentary mice, while structural properties remained unchanged, suggesting a decrease in bone quality despite increased bone quantity (46). Our data support a similar trend, whereby continuous HFS feeding dramatically increased cancellous bone mass and improved cancellous microarchitecture, as well as structural mechanical properties, while continuous LF feeding led to the highest values for material properties; though LF/LF and HFS/HFS+ mice did not exhibit statistically significant differences.

Despite significant alterations in microarchitecture, no differences were found between groups in relative osteoid surface, an index of bone formation, or in relative osteoclast surface, indicative of bone resorption. Mixed results are reported for relative osteoid and osteoclast or relative eroded surfaces after HF feeding in sedentary mice, showing both decreases and no differences in both parameters in LF-fed sedentary mice (4, 111). Only one study reported static histomophometric measures after HF feeding in exercising mice, demonstrating no difference in relative osteoblast or osteoclast surfaces between LF or HF (60% fat) for 14 weeks in exercising young male C57Bl/6 mice (73).

Few data exist on the impact of HFS feeding on osteocyte signaling, with no studies examining the added impact of exercise. The proportion of osteocytes positive for TNFα, sclerostin, and IGF-1 were similar across groups in both cancellous and cortical bone. Baek et al. reported significant increases in %+Ot-TNFα in both cancellous and cortical bone and in %+Ot-Scl in cortical bone after 12 weeks of 60% HF

feeding in young male mice (4). However, these mice were sedentary and also exhibited significant detriments to cancellous microarchitecture and cortical geometry, contrary to what we found. It is likely that the mechanical stimulus of exercise mitigates the inflammation-induced stimulus for bone resorption. Similarly, no differences were found in %+Ot-IGF-1, despite numerous studies showing elevated serum IGF-1 with HF feeding (46, 126). Interestingly, %+Ot-IFNγ was significantly lower in cancellous bone in mice continuously fed an HFS diet, consistent with data showing improved cancellous microarchitecture in this group. IFNγ has a complex mechanism of action and is capable of promoting osteogenic fates of mesenchymal stem cells while exerting a dual effect on osteoclast differentiation, such that at different stages IFNγ can either promote or inhibit osteoclast differentiation (110). IFNγ knock-out mice have decreased bone mass compared to controls, while IFNγ administration negatively impacts bone in vivo (110). Regular exercise stimulates production of IFNγ, increasing serum concentration, and is considered anti-inflammatory in this context (3). Given that, it is unclear why decreased IFNγ-osteocyte signaling is associated here with improvements in cancellous microarchitecture.

Increased marrow adiposity, a factor linked to increased bone fragility, specifically via upregulation of adipogenesis, is consistently reported with HF feeding in sedentary mice, post-weaning and after skeletal maturity (69, 94, 95, 111, 128). Switching to a LF diet after 12 weeks of HF feeding, prevents further infiltration of marrow adipocytes (95)s. Exercise, despite HF feeding, attenuates the diet-induced increase in marrow adiposity; even exercising LF-fed mice show attenuated adiposity

compared to sedentary counterparts (105, 106). Styner et al. showed no difference in adipocyte volume, number, or size between exercising LF and HF-fed mice (105). Interestingly, we found a significant increase in adipocyte size in exercising mice continuously fed the HFS diet versus mice continuously fed the LF diet. The primary differences between these studies are the use of 4-week-old female mice and a HF only diet, whereas we studied 5-week-old male mice and utilized a HF diet in combination with 20% fructose solution in place of regular drinking water. This led to significant increases in total body weight, fat mass, and caloric intake and decreases in physical activity not seen in studies utilizing only a HF diet.

We hypothesized that the addition of FMT's from healthy, exercising mice would have an additional beneficial bone impact when combined with diet alterations. However, we did not find any significant differences between HFS/LF+ and HFS/LF mice on most bone parameters. Interestingly, we did detect a differential response of combined diet alterations and FMT's on several intrinsic mechanical properties. This should be investigated further, particularly in sedentary mice where the absence of mechanical loading may result in a greater impact. As diet is the primary determinant of microbiota composition, alteration to a LF diet may have dominated the net impact on microbial composition (38, 47). Both exercise and obesity can directly modulate microbiota composition and these effects may have outweighed the impact of fecal microbial transplants in animals switched from the HFS to LF diet (114).

In sum, HFS feeding combined with exercise promotes bone anabolism and improves structural mechanical properties of the femur. Notably, altering diet from HFS

to LF appears to reverse improvements in cancellous microarchitecture and size-dependent properties of mechanical strength, likely as a result of short-term energy deficit. We found no detectable inflammatory impact on bone, suggesting exercise is protective in this context.

4. CONCLUSIONS

We sought to investigate whether an anti-inflammatory diet can reduce inflammation-mediated damage via irradiation to bone, as well as the ability for diet and microbiota supplementation to reverse the negative effects of a pro-inflammatory diet on bone.

We failed to detect a negative impact of radiation exposure on cancellous and cortical bone parameters, suggesting that radiation exposure may not lead to significant detriments to bone despite many findings in published literature to the contrary. Further research must be done to elucidate the impact of space-relevant radiation exposure by more closely mimicking GCR composition, total dosage, and dose rate. Caution should also be used when evaluating bone in animals matched for middle-aged humans, as low baseline cancellous bone volumes may prevent the detection of significant differences between treatment groups. A diet high in omega-3 fatty acids was able to successfully mitigate increased serum levels of TNFα across radiation doses, consistent with well-established literature. Interestingly, the FOP diet was only successful at reducing serum levels of TNFα at 4- and 8-weeks post exposure, highlighting that omega-3 fatty acids are beneficial for chronic, but not acute, inflammation. FOP-fed mice exhibited improved cancellous and cortical microarchitecture and geometry at 8 weeks post exposure to both ^{56}Fe and γ radiation, with improvements occurring at higher radiation doses; this occurred alongside an increased percentage of osteocytes staining positive for IGF-1, which is widely associated with bone anabolism. Further research is needed to

examine the impact of a diet high in omega-3 fatty acids to mitigate radiation-induced inflammation and potential bone loss in male mice, modulation to mitigate continuous, low dose and low dose-rate radiation in male and female mice, and combined continuous, low dose, low dose-rate radiation and simulated weightlessness in male and female mice. These studies should also focus on the coordinated cellular signaling response of osteocytes in these settings, as osteocytes are the primary regulatory bone cells and little information has been accumulated to date. Though much remains to be discovered, our first study provides important early evidence of a positive impact of radiation exposure, beneficial impacts of a diet high in omega-3 fatty acids on bone, and the cellular response of osteocytes to acute radiation exposure.

In the second experiment, we failed to detect a negative impact of HFS feeding on bone microarchitecture, geometry, and strength in exercising mice. In fact, HFS feeding combined with exercise promoted bone anabolism, improved femur structural properties; further, we found no detectable inflammatory impact on bone, suggesting exercise is protective in this context. However, the vast majority of obese individuals are sedentary and thus the impact of HFS feeding must also be evaluated in sedentary animals. Interestingly, HFS-fed exercising mice did not exhibit improved femur material properties, nor femoral neck strength, suggesting improved bone quantity, but not quality. Further research should evaluate the specific mechanisms by which bone quality is impacted with HFS feeding, in both sedentary and exercising mice. Despite minimal differences between the experimental groups assigned to diet alterations with and without fecal microbial transplants, these groups did exhibit a differential impact on

the femur material properties of ultimate stress and yield stress. The specific mechanisms by which microbiota and/or microbial transplants may alter bone material properties is an area of research with substantial therapeutic potential. Future research should evaluate the role of microbiota and/or microbial transplants on bone outcomes in sedentary and exercising mice exposed to HFS feeding. To date, no study has examined the impact of a high fat, high sugar diet and simulated sugar sweetened beverages on bone. As this diet most closely mimics a worse than average US citizen's diet, it is imperative to evaluate the long-term impacts on bone health and fracture risk.

In summary, dietary modulation of inflammation-mediated impacts on skeletal biology is a potential therapeutic target to protect against bone loss. We provide evidence for an anti-inflammatory diet to reduce systemic inflammation and modestly improve bone outcomes, supporting a role for diet to alter bone health. Interestingly, we showed a positive impact of diet-induced obesity on bone outcomes in exercising mice, providing a key role of exercise to outweigh impacts of "unhealthy" diets on bone health.

5. REFERENCES

1. **Alwood JS**, **Shahnazari M**, **Chicana B**, **Schreurs A**, **Kumar A**, **Bartolini A**, **Shirazi-Fard Y**, **Globus RK**. Ionizing Radiation Stimulates Expression of Pro-Osteoclastogenic Genes in Marrow and Skeletal Tissue Joshua. *J Interf Cytokine Res* 35, 2015.
2. **Alwood JS**, **Tran LH**, **Schreurs A-S**, **Shirazi-Fard Y**, **Kumar A**, **Hilton D**, **Tahimic CGT**, **Globus RK**. Dose- and Ion-Dependent Effects in the Oxidative Stress Response to Space-Like Radiation Exposure in Skeletal System. *Int J Mol Sci* 18, 2017.
3. **Ambarish V**, **Radhika K**. Alteration of Interferon Gamma (IFN-γ) in Human Plasma with Graded Physical Activity. *J Clin Diagnostic Res* 8: 13–15, 2014.
4. **Baek K**, **Hwang HYORIN**, **Park H**, **Kwon A**, **Qadir AS**, **Ko S**, **Woo KMI**, **Ryoo H**, **Kim G**, **Baek J**. TNF- a Upregulates Sclerostin Expression in Obese Mice Fed a High-Fat Diet. *J Cell Physiol* 229: 640–650, 2014.
5. **Bandstra ER**, **Pecaut MJ**, **Anderson ER**, **Willey JS**, **De Carlo F**, **Stock SR**, **Gridley DS**, **Nelson GA**, **Levine HG**, **Bate**. Long-Term Dose Response of Trabecular Bone in Mice to Proton Radiation. *Radiat Res* 169: 607–614, 2008.
6. **Bernstein CN**, **Blanchard JF**, **Leslie W**, **Wajda A**, **Yu BN**. The Incidence of Fracture among Patients with Inflammatory Bowel Disease. *Ann Intern Med* 133: 795–799, 2000.
7. **Bhattacharya A**, **Rahman M**, **Sun D**, **Fernandes G**. Effect of fish oil on bone mineral density in aging C57BL/6 female mice. *J Nutr Biochem* 18: 372–379,

2007.

8. **Bhattacharya A**, **Sun D**, **Rahman M**, **Fernandes G**. Different ratios of eicosapentaenoic and docosahexaenoic omega-3 fatty acids in commercial fish oils differentially alter pro-inflammatory cytokines in peritoneal macrophages from C57BL / 6 female mice. *J Nutr Biochem* 18: 23–30, 2007.
9. **Bokhari RS**. Skeletal Impacts of Continuous Low-Dose-Rate Gamma Radiation Exposure During Simulated Microgravity. 2018.
10. **Bokhari RS**, **Metzger CE**, **Black JM**, **Franklin KA**, **Boudreaux RD**, **Allen MR**, **Macias BR**, **Hogan HA**, **Braby LA**, **Bloom SA**. Positive impact of low-dose , high-energy radiation on bone in partial- and / or full-weightbearing mice. *npj Microgravity* 5: 1–9, 2019.
11. **Borchers AT**, **Keen CL**, **Gershwin ME**. Microgravity and Immune Responsiveness: Implications for Space Travel. *Nutrition* 18: 889–898, 2002.
12. **Bouxsein ML**, **Boyd SK**, **Christiansen BA**, **Guldberg RE**, **Jepsen KJ**, **Mu R**. Guidelines for Assessment of Bone Microstructure in Rodents Using Micro-Computed Tomography. *J Bone Miner Res* 25: 1468–1486, 2010.
13. **Boyce BF**, **Xing L**. Functions of RANKL/RANK/OPG in bone modeling and remodeling. *Arch Biochem Biophys* 473: 139–146, 2008.
14. **Bultink IEM**. Osteoporosis and Fractures in Systemic Lupus Erythematosus. *Arthritis Care Res (Hoboken)* 64: 2–8, 2012.
15. **Burr DB**, **Allen MR**, editors. *Basic and Applied Bone Biology*. 2nd Editio. Academic Press, 2019.

16. **Calder PC**. Dietary modification of inflammation with lipids. *Proc Nutr Soc* 61: 345–358, 2002.

17. **Calder PC**. n-3 Polyunsaturated fatty acids, inflammation, and inflammatory diseases. *Am J Clin Nutr* 83: 1505S–19S, 2006.

18. **Cao X**, **Wu X**, **Frassica D**, **Yu B**, **Pang L**, **Xian L**, **Wan M**, **Lei W**. Irradiation induces bone injury by damaging bone marrow microenvironment for stem cells. *PNAS* 108, 2011.

19. **Capulli M**, **Paone R**, **Rucci N**. Osteoblast and osteocyte : Games without frontiers. *Arch Biochem Biophys* 561: 3–12, 2014.

20. **Center for Disease Control National Center for Health Statistics**. *Diet/Nutrition*. [date unknown].

21. **Chandra A**, **Lin T**, **Young T**, **Tong W**, **Ma X**, **Tseng W**, **Kramer I**, **Kneissel M**, **Levine MA**, **Zhang Y**, **Cengel K**, **Liu XS**, **Qin L**. Suppression of Sclerostin Alleviates Radiation-Induced Bone Loss by Protecting Bone-Forming Cells and Their Progenitors Through Distinct Mechanisms. *J Bone Miner Res* 32: 360–372, 2017.

22. **Crockett JC**, **Mellis DJ**, **Scott DI**, **Helfrich MH**. New knowledge on critical osteoclast formation and activation pathways from study of rare genetic diseases of osteoclasts : focus on the RANK / RANKL axis RB. *Osteoporos Int* 22: 1–20, 2011.

23. **Crucian BE**, **Zwart SR**, **Mehta S**, **Uchakin P**, **Quiriarte HD**, **Pierson D**, **Sams CF**, **Smith SM**. Plasma Cytokine Concentrations Indicate That In Vivo Hormonal

Regulation of Immunity Is Altered During Long-Duration Spaceflight. *J Interf Cytokine Res* 34: 778–786, 2014.

24. **Davidson SR**, **Burnett M**, **Hoffman-goetz L**. Training Effects in Mice after Long-Term Voluntary Exercise. *Med Sci Sport Exerc* 38: 250–255, 2006.

25. **Dehghan M**, **Akhtar-danesh N**, **Merchant AT**. Childhood obesity, prevalence and prevention. *Nutrition* 8: 1–8, 2005.

26. **Donahue SMA**, **Rifas-shiman SL**, **Gold DR**, **Jouni ZE**, **Gillman MW**, **Oken E**. Prenatal fatty acid status and child adiposity at age 3 y: results from a US pregnancy cohort. *Am J Clin Nutr* 93: 780–788, 2011.

27. **Doucette CR**, **Horowitz MC**, **Berry R**, **Macdougald OA**, **Anunciado-koza REA**, **Koza RA**. A High Fat Diet Increases Bone Marrow Adipose Tissue (MAT) But Does Not Alter Trabecular or Cortical Bone Mass in C57BL / 6J Mice. *J Cell Physiol* : 2032–2037, 2015.

28. **Doucette CR**, **Horowitz MC**, **Berry R**, **Macdougald OA**, **Anunciado-koza REA**, **Koza RA**. A High Fat Diet Increases Bone Marrow Adipose Tissue (MAT) But Does Not Alter Trabecular or Cortical Bone Mass in C57BL / 6J Mice. : 2032–2038, 2015.

29. **Eikelbloom R**. Human parallel to voluntary wheel running: exercise. *Anim Behav* 57: F11–F12, 1999.

30. **Ergun H**, **Howland W**. Postradiation atrophy of mature bone. *CRC Crit Rev Diagn Imaging* 12: 225–43, 1980.

31. **Fakhry M**, **Hamade E**, **Badran B**, **Buchet R**, **Magne D**. Molecular mechanisms

of mesenchymal stem cell differentiation towards osteoblasts. *World J Stem Cells* 5: 136–148, 2013.

32. **Felice JI**, **Gangoiti MV**, **Molinuevo MS**, **McCarthy AD**, **Cortizo AM**. Effects of a metabolic syndrome induced by a fructose-rich diet on bone metabolism in rats. *Metabolism* 63: 296–305, 2014.

33. **Florencio-silva R**, **Rodrigues G**, **Sasso-cerri E**, **Simões MJ**, **Cerri PS**, **Cells B**. Biology of Bone Tissue : Structure , Function , and Factors That Influence Bone Cells. *Biomed. Res. Int.* .

34. **Franz-odendaal TA**, **Hall BK**, **Witten PE**. Buried Alive: How Osteoblasts Become Osteocytes. *Dev Dyn* 235: 176–190, 2006.

35. **Glatt V**, **Canalis E**, **Stadmeyer L**, **Bouxsein ML**. Age-Related Changes in Trabecular Architecture Differ in Female and Male C57Bl/6J Mice. *J Bone Miner Res* 22, 2007.

36. **Goulding A**, **Taylor RW**, **Jones IE**, **McAuley KA**, **Manning PJ**, **Williams SM**. Overweight and obese children have low bone mass and area for their weight. *Int J Obes* 24: 627–632, 2000.

37. **Gueguinou N**, **Huin-Schohn C**, **Bascove M**, **Bueb J-L**, **Tschirhart E**, **Legrand-Frossi C**, **Frippiat J-P**. Could spaceflight-associated immune system weakening preclude the expansion of human presence beyond Earth' s orbit ? *J Leukoc Biol* 86: 1027–1038, 2009.

38. **Guss JD**, **Hors MW**, **Fontenele FF**, **Sandoval TN**, **Luna M**, **Apoorva F**, **Lima SF**, **Bicalho RC**, **Singh A**, **Ley RE**, **Meulen MCH Van Der**, **Goldring SR**,

Hernandez CJ. Alterations to the Gut Microbiome Impair Bone Strength and Tissue Material Properties. *J Bone Miner Res* 32: 1343–1353, 2017.

39. **Hales CM**, **Carroll MD**, **Fryar CD**, **Ogden CL**. Prevalence of Obesity Among Adults and Youth: United States, 2015–2016 Key findings Data from the National Health and Nutrition Examination Survey [Online]. *Natl Cent Heal Stat* 1: 1–8, 2017. https://www.cdc.gov/nchs/data/databriefs/db288.pdf.

40. **Hall EJ**, **Giaccia AJ**. *Radiobiology for the Radiologist*. 2006.

41. **Hamilton S**, **Pecaut MJ**, **Gridley DS**, **Travis ND**, **Bandstra ER**, **Willey JS**, **Nelson GA**, **Bateman TA**. A murine model for bone loss from therapeutic and space-relevant sources of radiation. *J Appl Physiol* 101: 789–793, 2006.

42. **Hardy R**, **Cooper MS**. Bone loss in inflammatory disorders. *J Endocrinol* 201: 309–320, 2009.

43. **Hofbauer LC**, **Lacey DL**, **Dunstan CR**, **Spelsberg TC**, **Riggs BL**, **Khosla S**. Interleukin-1B and Tumor Necrosis Factor-a, But Not Interleukin-6, Stimulate Osteoprotegerin Ligand Gene Expression in Human Osteoblastic Cells. *Bone* 25: 255–259, 1999.

44. **Holguin N**, **Brodt MD**, **Sanchez ME**, **Silva MJ**. Aging diminishes lamellar and woven bone formation induced by tibial compression in adult C57BL/6. *Bone* 65: 83–91, 2014.

45. **Hou JC**, **Zernicke F**, **Barnard J**. Hiah fat-sucrose diet effects on femoral neck b hanics. *Clin Biomech* 5: 162–168, 1990.

46. **Ionova-martin SS**, **Do SH**, **Barth HD**, **Szadkowska M**, **Porter AE**, **Iii JWA**, **Jr**

JWA, **Alliston T**, **Vaisse C**, **Ritchie RO**. Reduced size-independent mechanical properties of cortical bone in high-fat diet-induced obesity. *Bone* 46: 217–225, 2010.

47. **Jones RM**, **Mulle JG**, **Paci R**. Osteomicrobiology: The influence of gut microbiota on bone in health and disease. *Bone* 115: 59–67, 2018.

48. **Kaneki H**, **Guo R**, **Chen D**, **Yao Z**, **Schwarz EM**, **Zhang YE**, **Boyce BF**, **Xing L**. Tumor Necrosis Factor Promotes Runx2 Degradation through Up-regulation of Smurf1 and Smurf2 in Osteoblasts. *J Biol Chem* 281: 4326–4333, 2006.

49. **Kelley D**, **Taylor P**, **Nelson G**, **Schmidt PC**, **Ferretti A**, **Erickson KL**, **Yu R**, **Chandra RK**, **Mackey BE**. Docosahexaenoic Acid Ingestion Inhibits Natural Killer Cell Activity and Production of Inflammatory Mediators in Young Healthy Men. *Lipids* 34: 1–8, 1999.

50. **Kinsella J**, **Lokesh B**, **Broughton S**, **Whelan J**. Dietary polyunsaturated fatty acids and eicosanoids: potential effects on the modulation of inflammatory and immune cells: an overview. *Nutrition* 6: 24–44, 1990.

51. **Klaus J**, **Armbrecht G**, **Steinkamp M**, **Bruckel J**, **Rieber A**, **Adler G**, **Reinshagen M**, **Felsenberg D**, **Tirpitz C Von**. High prevalence of osteoporotic vertebral fractures in patients with Crohn's disease. *Gut* 51: 654–658, 2002.

52. **Kobayashi BK**, **Takahashi N**, **Jimi E**, **Udagawa N**, **Takami M**, **Kotake S**, **Nakagawa N**, **Kinosaki M**, **Yamaguchi K**, **Shima N**, **Yasuda H**, **Morinaga T**, **Higashio K**, **Martin TJ**, **Suda T**. Tumor Necrosis Factor ␣ Stimulates Osteoclast Differentiation by a Mechanism Independent of the ODF / RANKL –

RANK Interaction. *J Exp Med* 191, 2000.

53. **Kondo H**, **Yumoto K**, **Alwood JS**, **Mojarrab R**, **Wang A**, **Almeida EAC**, **Searby ND**, **Limoli CL**, **Globus RK**. Oxidative stress and gamma radiation-induced cancellous bone loss with musculoskeletal disuse. *J Appl Physiol* 108: 152–161, 2010.

54. **Kromhout D**, **Goede J De**. Update on cardiometabolic health effects of w-3 fatty acids. *Curr Opin Lipidol* 25: 85–90, 2014.

55. **de la Serre CB**, **Ellis CL**, **Lee J**, **Hartman AL**, **Rutledge JC**, **Raybould HE**. Propensity to high-fat diet-induced obesity in rats is associated with changes in the gut microbiota and gut inflammation. *Am J Physiol Gastrointest Liver Physiol* 229: 440–448, 2010.

56. **Lam J**, **Ross FP**, **Teitelbaum SL**, **Lam J**, **Takeshita S**, **Barker JE**, **Kanagawa O**, **Ross FP**, **Teitelbaum SL**. TNF-a induces osteoclastogenesis by direct stimulation of macrophages exposed to permissive levels of RANK ligand Find the latest version : TNF- α induces osteoclastogenesis by direct stimulation of macrophages exposed to permissive levels of RANK ligand. *J Clin Investig* 106: 1481–1488, 2000.

57. **Lang T**, **Leblanc A**, **Evans H**, **Lu Y**, **Genant H**, **Yu A**. Cortical and Trabecular Bone Mineral Loss From the Spine and Hip in Long-Duration Spaceflight. *J Bone Miner Res* 19, 2004.

58. **Lang T**, **Van Loon JJWA**, **Bloomfield S**, **Vico L**, **Chopard A**, **Rittweger J**, **Kyparos A**, **Blottner D**, **Vuori I**, **Gerzer R**, **Cavanagh PR**. Towards human

exploration of space: the THESEUS review series on muscle and bone research priorities. *npj Microgravity* 3: 8, 2017.

59. **Lang TF**, **Leblanc AD**, **Evans HJ**, **Lu Y**. Adaptation of the Proximal Femur to Skeletal Reloading After Long-Duration Spaceflight. *J Bone Miner Res* 21: 1224–1230, 2006.

60. **LeBlanc A**, **Matsumoto T**, **Jones J**, **Shapiro J**, **Lang T**, **Shackelford L**, **Smith SM**, **Evans H**, **Spector E**, **Ploutz-Snyder R**, **Sibonga J**, **Keyak J**, **Nakamura T**, **Kohri K**, **Ohshima H**. Bisphosphonates as a supplement to exercise to protect bone during long-duration spaceflight. *Osteoporos Int* 24: 2105–2114, 2013.

61. **Leblanc A**, **Schneider V**, **Shackelford L**, **West S**, **Oganov V**, **Bakulin A**, **Voronin L**. Bone mineral and lean tissue loss after long duration space flight. *J Musculoskel Neuron Intact* 1: 157–160, 2000.

62. **Lee TH**, **Shihii C**, **Coreyll EJ**, **Lewis RA**, **Austens KF**. Characterization and Biologic Properties of 5,12-Dihydroxy Derivatives of Eicosapentaenoic Acid, Including Leukotriene B5 and the Double Lipoxygenase Product. *J Biol. Chem.* .

63. **Letsinger AC**. The Evolution & Regulation of Physical Activity Levels. 2019.

64. **Li C**, **Huang Q**, **Yang R**, **Dai Y**, **Zeng Y**, **Tao L**, **Li X**, **Zeng J**, **Wang Q**. Gut microbiota composition and bone mineral loss — epidemiologic evidence from individuals in Wuhan , China. *Osteoporos Int* 30: 1003–1013, 2019.

65. **Li L**, **Rao S**, **Cheng Y**, **Zhuo X**, **Deng C**, **Xu N**, **Zhang H**. Microbial osteoporosis: The interplay between the gut microbiota and bones via host metabolism and immunity. *Microbiology* : 1–15, 2019.

66. **Lima F**, **Swift JM**, **Greene ES**, **Allen MR**, **Cunningham DA**, **Leslie A**. Exposure to Low-Dose X-Ray Radiation Alters Bone Progenitor Cells and Bone Microarchitecture. *Radiat Res* 188: 433–442, 2017.

67. **Lloyd SAJ**, **Bandstra ER**, **Travis ND**, **Nelson GA**, **Daniel J**, **Pecaut MJ**, **Gridley DS**, **Willey JS**, **Bateman TA**. Spaceflight-relevant types of ionizing radiation and cortical bone: Potential LET effect? *Adv Sp Res* 42: 1889–1897, 2009.

68. **Lo C**, **Chiu KC**, **Fu M**, **Lo R**, **Helton S**. Fish Oil Decreases Macrophage Tumor Necrosis Factor Gene Transcription by Altering the NFkB. *J Surg Res* 82: 216–221, 1999.

69. **Lu XMEI**, **Zhao H**, **Wang ENHUA**. A high-fat diet induces obesity and impairs bone acquisition in young male mice. *Mol Med Rep* 7: 1203–1208, 2013.

70. **Macias BR**, **Lima F**, **Swift JM**, **Shirazi-fard Y**, **Greene ES**, **Allen MR**, **Fluckey J**, **Hogan HA**. Simulating the Lunar Environment : Partial Weightbearing and High-LET Radiation-Induce Bone Loss and Increase Sclerostin-Positive Osteocytes. *Radiat Res* 263: 254–263, 2016.

71. **McCabe LR**, **Irwin R**, **Schaefer L**, **Britton RA**. Probiotic Use Decreases Intestinal Inflammation and Increases Bone Density in Healthy Male but not Female Mice. *J Cell Physiol* 228: 1793–1798, 2013.

72. **Mccabe LR**, **Irwin R**, **Tekalur A**, **Evans C**, **Schepper JD**. Exercise prevents high fat diet-induced bone loss , marrow adiposity and dysbiosis in male mice. *Bone* 118: 20–31, 2019.

73. **McCabe LR**, **Irwin R**, **Tekalur A**, **Evans C**, **Schepper JD**. Exercise prevents high fat diet-induced bone loss , marrow adiposity and dysbiosis in male mice. *Bone* : 0–1, 2018.

74. **Medina-Gomez C**. Bone and the gut microbiome : a new dimension. *J Lab Precis Med* 3: 1–10, 2018.

75. **Metzger CE**, **Brezicha JE**, **Elizondo JP**, **Narayanan SA**, **Hogan HA**, **Bloom SA**. Differential responses of mechanosensitive osteocyte proteins in fore- and hindlimbs of hindlimb-unloaded rats. *Bone* 105: 26–34, 2017.

76. **Metzger CE**, **Narayanan SA**. The Role of Osteocytes in Inflammatory Bone Loss. *Front Endocrinol (Lausanne)* 10: 1–7, 2019.

77. **Miriam B. Vos, MD, MSPH, Joel E. Kimmons, Cathleen Gillespie, MS, Jean Welsh, MPH, RN, Heidi Michels Blanck P**. Dietary Fructose Consumption Among US Children and Adults: The Third National Health and Nutrition Examination Survey. *Medscape J Med* 10, 2008.

78. **Mitchell MJ**, **Logan PM**. Radiation-induced Changes in Bone. *Radiographics* 18: 1125–1136, 1998.

79. **Mozaffarian D**, **Rimm EB**. Fish Intake, Contaminants, and Human Health. *J Am Med Assoc* 296: 1885–1900, 2006.

80. **Multhoff G**, **Radons J**, **Gaipl US**. Radiation, inflammation, and immune responses in cancer. *Front Oncol* 2: 1–18, 2012.

81. **Nakanishi A**, **Iitsuka N**, **Tsukamoto I**. Fish oil suppresses bone resorption by inhibiting osteoclastogenesis through decreased expression of M-CSF , PU.1 ,

MITF and RANK in ovariectomized rats. *Mol Med Rep* 7: 1896–1903, 2013.

82. **Nanes MS**. Tumor necrosis factor- a : molecular and cellular mechanisms in skeletal pathology. *Gene* 321: 1–15, 2003.

83. **NASA**. *Space Radiation*. 2018.

84. **National Council on Radiation Protection and Measurements**. *Information Needed to Make Radiation Protection Recommendations for Space Missions Beyond Low-Earth Orbit.* Bethesda, MD: 2006.

85. **Nettleton JA**, **Katz R**. n-3 Long-Chain Polyunsaturated Fatty Acids in Type 2 Diabetes: A Review. *J Am. Diabet. Assoc.* (2005). doi: 10.1016/j.jada.2004.11.029.

86. **Novak TE**, **Babcock TA**, **Jho DH**, **Helton WS**, **Espat NJ**, **Novak TE**, **Babcock TA**, **Jho DH**, **Helton WS**, **Espat NJ**, **Helton S**, **Espat NJ**, **Nf- B**. NF- κB inhibition by ω -3 fatty acids modulates LPS-stimulated macrophage TNF-α transcription. *Am J Physiol Lung Cell Mol Physiol* 284: L84–L89, 2002.

87. **Overgaard M**. Spontaneous Radiation-Induced Rib Fractures in Breast Cancer Patients Treated with Postmastectomy Irradiation — A Clinical Radiobiological Analysis of the Influence of Fraction Size and Dose-Response Relationships on Late Bone Damage. *Acta Oncol (Madr)* 27: 117–122, 2009.

88. **Parlee SD**, **Lentz SI**, **Mori H**, **Macdougald OA**. Quantifying Size and Number of Adipocytes in Adipose Tissue. *Methods Enzym* 537: 93–122, 2014.

89. **Pollock, Norman K, Laing, Emma M, Baile, Clifton A, Hamrick, Mark W, Hall, Daniel B, Lewis RD**. Is adiposity advantageous for bone strength? A

peripheral quantitative computed tomography study in late adolescent females [Online]. *Am J Clin Nutr* 86: 1530–8., 2007. http://www.scopus.com/inward/record.url?eid=2-s2.0-36249021055&partnerID=40&md5=191b10560dba52e4b5a07991bd4d5a9f.

90. **Ponzetti M**, **Rucci N**. Updates on Osteoimmunology : What's New on the Cross-Talk Between Bone and Immune System. *Front Endocrinol (Lausanne)* 10: 1–13, 2019.

91. **Rohrer MD**, **Arbor A**. The effect of cobalt-60 irradiation on monkey mandibles. *Oral Surg Oral Med Oral Pathol* 48: 424–440, 1979.

92. **Romieu I**, **Dossus L**, **Barquera S**, **Blottière HM**, **Franks PW**, **Gunter M**, **Hwalla N**, **Hursting SD**, **Leitzmann M**, **Margetts B**, **Nishida C**, **Potischman N**, **Seidell J**, **Stepien M**, **Wang Y**, **Westerterp K**, **Winichagoon P**, **Wiseman M**, **Willett WC**. Energy balance and obesity: what are the main drivers? *Cancer Causes Control* 28: 247–258, 2017.

93. **Sakaguchi K**, **Morita I**, **Murota S**. Eicosapentaenoic Acid Inhibits Bone Loss Due to Ovariectomy in Rats. *Prostoglandins, Leukot Essent Fat Acids* 50: 81–84, 1994.

94. **Scheller EL**, **Doucette CR**, **Learman BS**, **Cawthorn WP**, **Khandaker S**, **Schell B**, **Wu B**, **Ding S**, **Bredella MA**, **Fazeli PK**, **Khoury B**, **Jepsen KJ**, **Pilch PF**, **Klibanski A**, **Rosen CJ**, **Macdougald OA**. Region-specific variation in the properties of skeletal adipocytes reveals regulated and constitutive marrow adipose tissues. *Nat Commun* 6: 1–13, 2015.

95. **Scheller EL**, **Khoury B**, **Moller KL**, **Wee NKY**, **Scheller EL**. Changes in Skeletal Integrity and Marrow Adiposity during High-Fat Diet and after Weight Loss. *Front Endocrinol (Lausanne)* 7: 1–13, 2016.

96. **Schreurs A**, **Shahnazari M**, **Alwood JS**, **Truong TA**, **Tahimic CGT**. Dried plum diet protects from bone loss caused by ionizing radiation. *Nat Publ Gr* : 1–11, 2016.

97. **Seeman E**, **Delmas PD**. Bone Quality — The Material and Structural Basis of Bone Strength and Fragility. *N Engl J Med* 354: 2250–2261, 2006.

98. **Shapses SA**, **Pop LC**, **Wang Y**. Obesity is a concern for bone health with aging. *Nutr Res* 39: 1–13, 2017.

99. **Simopoulos AP**. Omega-3 Fatty Acids in Inflammation and Autoimmune Diseases. *J Am Coll Nutr* 21: 495–505, 2002.

100. **Simopoulos AP**. Experimental Biology and Medicine The Importance of the Omega-6 / Omega-3 Fatty Acid Ratio in Cardiovascular Disease and Other Chronic Diseases. *Exp Biol Med* 233, 2008.

101. **Simopoulos AP**. Dietary Omega-3 Fatty Acid Deficiency and High Fructose Intake in the Development of Metabolic Syndrome, Brain Metabolic Abnormalities, and Non-Alcoholic Fatty Liver Disease. *Nutrients* (2013). doi: 10.3390/nu5082901.

102. **Simopoulos AP**, **Gene O**. An Increase in the Omega-6 / Omega-3 Fatty Acid Ratio Increases the Risk for Obesity. *Nutrients* 8: 1–17, 2016.

103. **Sjorgen K**, **Engdahl C**, **Henning P**, **Lerner UH**, **Tremaroli V**, **Lagerquist MK**,

Ba F. The Gut Microbiota Regulates Bone Mass in Mice. *J Bone Miner Res* 27: 1357–1367, 2012.

104. **Staa TP Van**, **Geusens P**, **Bijlsma JWJ**, **Leufkens HGM**, **Cooper C**. Clinical Assessment of the Long-Term Risk of Fracture in Patients With Rheumatoid Arthritis. *Arthritis Rheum* 54: 3104–3112, 2006.

105. **Styner M**, **Pagnotti GM**, **McGrath C**, **Wu X**, **Sen B**, **Uzer G**, **Xie Z**, **Zong X**, **Styner MA**, **Rubin CT**, **Rubin J**. Exercise Decreases Marrow Adipose Tissue Through ß-Oxidation in Obese Running Mice. *J Bone Miner Res* 32: 1692–1702, 2017.

106. **Styner M**, **Thompson WR**, **Galior K**, **Uzer G**, **Wu X**, **Kadari S**, **Case N**, **Xie Z**, **Sen B**, **Romaine A**, **Pagnotti GM**, **Rubin CT**, **Styner MA**, **Horowitz MC**, **Rubin J**. Bone marrow fat accumulation accelerated by high fat diet is suppressed by exercise. *Bone* 64: 39–46, 2014.

107. **Suman S**, **Kumar S**, **Jr AJF**, **Datta K**. Space radiation exposure persistently increased leptin and IGF1 in serum and activated leptin-IGF1 signaling axis in mouse intestine. *Nat Sci Reports* 6: 1–11, 2016.

108. **Sun D**, **Krishnan A**, **Zaman K**, **Lawrence R**, **Bhattacharya A**, **Fernandes G**. Dietary n-3 Fatty Acids Decrease Osteoclastogenesis and Loss of Bone Mass In Ovariectomized Mice. *J Bone Miner Res* 18, 2003.

109. **Takayanagi H**. Osteoimmunology: shared mechanisms and crosstalk between the immune and bone systems. *Nat Rev Immunol* 7, 2007.

110. **Tang M**, **Tian L**, **Luo G**, **Yu X**. Interferon-Gamma-Mediated Osteoimmunology.

Front Immunol 9, 2018.

111. **Tencerova M**, **Figeac ÃF**, **Ditzel ÃN**, **Taipaleenm H**, **Nielsen TK**. High-Fat Diet – Induced Obesity Promotes Expansion of Bone Marrow Adipose Tissue and Impairs Skeletal Stem Cell Functions in Mice. *J Bone Miner Res* 33: 1154–1165, 2018.

112. **Tian L**, **Wang C**, **Xie Y**, **Wan S**, **Zhang K**, **Yu X**. High fructose and high fat exert different effects on changes in trabecular bone micro-structure. *J Nutr Heal Aging* 22: 361–370, 2018.

113. **Tilley SL**, **Coffman TM**, **Koller BH**, **Tilley SL**, **Coffman TM**, **Koller BH**. Mixed messages : modulation of inflammation and immune responses by prostaglandins and thromboxanes Find the latest version : Mixed messages : modulation of inflammation and immune responses by prostaglandins and thromboxanes. *J Clin Investig* 108: 15–23, 2001.

114. **Tremaroli V**, **Backhed F**. Functional interactions between the gut microbiota and host metabolism. *Nature* 489: 1–8, 2012.

115. **Turner CH**. Biomechanics of Bone: Determinants of Skeletal Fragility and Bone Quality. *Osteoporos Int* 13: 97–104, 2002.

116. **Uhlen M**, **Oksvold P**, **Fagerber L**, **Lundberg E**, **Jonasson K**, **Forsber M**, **Zwahlen M**, **Kampf C**, **Wester K**, **Hober S**, **Wernerus H**, **Bjorling L**, **Ponten F**. Towards a knowledge-based Human Protein Atlas [Online]. *Nat Biotechnol* 28: 1248–1250, 2010. www.proteinatlas.org.

117. **Vico L**, **Collet P**, **Guignandon A**, **Thomas T**, **Rehailia M**. Effects of long-term

microgravity exposure on cancellous and cortical weight-bearing bones of cosmonauts. *Lancet* 355, 2000.

118. **Wall R**, **Ross RP**, **Fitzgerald GF**, **Stanton C**. Fatty acids from fish: the anti-inflammatory potential of long-chain omega-3 fatty acids. *Nutr Rev* 68: 280–289, 2010.

119. **Watkins BA**, **Li Y**, **Lippman HE**, **Feng S**. Modulatory effect of omega-3 polyunsaturated fatty acids on osteoblast function and bone metabolism. *Prostoglandins, Leukot Essent Fat Acids* 68: 387–398, 2003.

120. **Weaver CM**. Diet, Gut Microbiome, and Bone Health. *Curr Osteoporos Rep* 13: 125–130, 2015.

121. **Willey JS**, **Grilly LG**, **Howard SH**, **Pecaut MJ**, **Obenaus A**, **Gridley DS**, **Nelson GA**. Bone Architectural and Structural Properties after 56 Fe 26+ Radiation-Induced Changes in Body Mass. *Radiat Res* 170: 201–207, 2008.

122. **Willey JS**, **Lloyd SAJ**, **Nelson GA**, **Bateman TA**. Space Radiation and Bone Loss. *Gravit Sp Biol Bull* 25: 14–21, 2012.

123. **Willey JS**, **Lloyd SAJ**, **Nelson GA**, **Linda L**, **Bateman TA**. Ionizing Radiation and Bone Loss: Space Exploration and Clinical Therapy Applications. *Clin Rev Bone Min Metab* 9: 54–62, 2012.

124. **Willey JS**, **Lloyd SAJ**, **Robbins ME**, **Bourland JD**, **Smith- H**, **Bowman LC**, **Norrdin RW**, **Bateman TA**. Early Increase in Osteoclast Number in Mice after Whole-Body Irradiation with 2 Gy X Rays. *Radiat Res* 170: 388–392, 2008.

125. **Williams HJ**, **Davies AM**. The effect of X-rays on bone: a pictorial review. *Eur*

Radiol 16: 619–633, 2006.

126. **Wu S**, **Aguilar AL**, **Ostrow V**, **Luca F De**. Insulin Resistance Secondary to a High-Fat Diet Stimulates Longitudinal Bone Growth and Growth Plate Chondrogenesis in Mice. *J Endocrinol* 152: 468–475, 2011.

127. **Yan J**, **Charles JF**. Gut Microbiome and Bone: To Build, Destory, or Both? *Curr Osteoporos Rep* 15: 376–384, 2017.

128. **Yarrow JF**, **Toklu HZ**, **Balaez A**, **Phillips EG**, **Otzel DM**, **Chen C**, **Wronski TJ**, **Ignacio Aguerre J**, **Sakarya Y**, **Tumer N**, **Scarpace PJ**. Fructose Consumption Does Not Worsen Bone Deficits Resulting From High-Fat Feeding in Young Male Rats Joshua. *BoneBone* 85: 99–106, 2017.

129. **Yumoto K**, **Globus RK**, **Mojarrab R**, **Arakaki J**, **Wang A**, **Searby ND**, **Almeida EAC**, **Limoli CL**. Short-Term Effects of Whole-Body Exposure to 56Fe Ions in Combinatio with Musculoskeletal Disuse on Bone Cells. *Radiat Res* 173: 494–504, 2010.

130. **Zernicke RF**, **Salem GJ**, **Barnard RJ**, **Schramm E**. Long-Term, High-Fat-Sucrose Diet Alters Rat Femoral Neck and Vertebral Morphology, Bone Mineral Content, and Mechanical Properties. *Bone* 16: 25–31, 1995.

131. **Zhao L**, **Jiang H**, **Papasian CJ**, **Maulik D**, **Drees B**, **Hamilton J**, **Deng H**. Correlation of Obesity and Osteoporosis: Effect of Fat Mass on the Determination of Osteoporosis. *J Bone Miner Res* 23, 2008.

132. **Zhao Y**, **Joshi-barve S**, **Barve S**, **Chen LH**, **Zhao Y**, **Ph D**, **Joshi-barve S**, **Ph D**, **Barve S**, **Ph D**, **Chen LH**, **Ph D**. Eicosapentaenoic Acid Prevents LPS-

Induced TNF-α Expression by Preventing NF- κB Activation. *J Am Coll Nutr* 23: 71–78, 2004.

133. **Zwart SR**, **Pierson D**, **Mehta S**, **Gonda S**, **Smith SM**. Capacity of Omega-3 Fatty Acids or Eicosapentaenoic Acid to Counteract Weightlessness-Induced Bone Loss by Astronauts. *J Bone Miner Res* 25: 1049–1057, 2010.